



# CHORUS

This is the accepted manuscript made available via CHORUS. The article has been published as:

## High transverse momentum quarkonium production and dissociation in heavy ion collisions

Rishi Sharma and Ivan Vitev

Phys. Rev. C **87**, 044905 — Published 15 April 2013

DOI: [10.1103/PhysRevC.87.044905](https://doi.org/10.1103/PhysRevC.87.044905)

# High transverse momentum quarkonium production and dissociation in heavy ion collisions

Rishi Sharma<sup>1\*</sup> and Ivan Vitev<sup>2†</sup>

<sup>1</sup> *TRIUMF, Theory Group, 4004 Wesbrook Mall, Vancouver, Canada and*

<sup>2</sup> *Los Alamos National Laboratory, Theoretical Division, Los Alamos, NM 87545, USA*

We calculate the yields of quarkonia in heavy ion collisions at RHIC and the LHC as a function of their transverse momentum. Based upon non-relativistic quantum chromodynamics, our results include both color-singlet and color-octet contributions and feed-down effects from excited states. In reactions with ultra-relativistic nuclei, we focus on the consistent implementation of dynamically calculated nuclear matter effects, such as coherent power corrections, cold nuclear matter energy loss, and the Cronin effect in the initial state. In the final state, we consider radiative energy loss for the color-octet state and collisional dissociation of quarkonia as they traverse through the QGP. Theoretical results are presented for  $J/\psi$  and  $\Upsilon$  and compared to experimental data where applicable. At RHIC, a good description of the high- $p_T$   $J/\psi$  modification observed in central Cu+Cu and Au+Au collisions can be achieved within the model uncertainties. We find that measurements of  $J/\psi$  yields in proton-nucleus reactions are needed to constrain the magnitude of cold nuclear matter effects. At the LHC, a good description of the experimental data can be achieved only in mid-central and peripheral Pb+Pb collisions. The large five-fold suppression of prompt  $J/\psi$  in the most central nuclear reactions may indicate for the first time possible thermal effects at the level of the quarkonium wavefunction at large transverse momenta.

PACS numbers: 12.38.Bx; 12.39.Ki; 13.87.Fh; 24.85.+p

## I. INTRODUCTION

Melting of heavy quarkonium states, like the  $J/\psi$  and the  $\Upsilon$ , due to color screening in a deconfined quark-gluon plasma (QGP) [1] has been proposed as one of the principal signatures for its formation. An expected experimental consequence of this melting in the thermal medium created in heavy ion collisions (HIC) is a suppression of the yields of heavy mesons, when compared to their yields in nucleon-nucleon (NN) collisions scaled with the number of binary interactions.

In a simplified picture, one can think of a quarkonium as a  $Q\bar{Q}$  pair in a color-singlet bound state, where the heavy quark ( $Q$ ) and the anti-quark ( $\bar{Q}$ ) are separated by distances  $\sim 1/(m_Q v)$ , smaller than  $1/\Lambda_{QCD}$ . Here,  $v \sim \alpha_s(m_Q v)$  is the relative velocity between  $Q$  and  $\bar{Q}$ , and the state is held together by an effective potential interaction. The sizes of the higher excited states are larger, and the sizes of the bottomonia are smaller than the corresponding charmonia. The presence of a thermal medium screens the interactions between the  $Q$  and  $\bar{Q}$  and leads to melting at some characteristic temperature [2] that depends on the meson. This picture suggests that it may be possible to observe sequential melting of narrower quarkonia as we explore thermal media of increasing temperatures [3, 4]. Several studies (see [5] for a recent review) have calculated the modification of quarkonium yields in collisions at SPS, RHIC, and the LHC [6–11].

A more sophisticated description of quarkonia is provided by non-relativistic quantum chromodynamics (NRQCD) [12]. In this picture, the  $Q\bar{Q}$  state in the color-singlet combination is the lowest order Fock space component of the full quarkonium wavefunction. Higher Fock components in the wavefunction have additional partons and are suppressed by positive powers of the small parameter  $v$ . In our calculation we will take into account both color-singlet

---

\*Electronic address: rishi@triumf.ca

†Electronic address: ivitev@lanl.gov

and color-octet  $Q\bar{Q}$  contributions in the production. The NRQCD formalism has been used to calculate differential yields of heavy mesons as a function of their transverse momentum,  $p_T$ , in p+p collisions [12–16]. The picture of the production process in NRQCD is as follows. The initial hard collision produces a “proto-quarkonium”, a short distance ( $\sim 1/m_Q$ )  $Q\bar{Q}$  pair where the  $Q$  and the  $\bar{Q}$  can be in the color-singlet or the octet state. Since this process is short-distance, it can be calculated using perturbative QCD [17]. This “proto-quarkonium” then evolves into the quarkonium state with probabilities that are given by non-perturbative matrix elements. For color-octet states, this evolution process also involves the emission of soft partons to form a net color-singlet object. The final state thus formed has a hierarchy of Fock space components that are given by NRQCD scaling rules. In this paper, we combine the NRQCD formalism with cold nuclear matter (CNM) effects and the effects of propagation of quarkonia through a hot QGP to calculate the final yields in HIC. We then obtain the nuclear modification ratio,

$$R_{AB}(p_T; N_{\text{part}}) = \frac{d\sigma_{AB}^{Q\bar{Q}}/dydp_T}{N_{AB}^{\text{coll}} d\sigma_{pp}^{Q\bar{Q}}/dydp_T}, \quad (1)$$

in reactions with heavy nuclei. In Eq. 1,  $N_{\text{part}}$  refers to the number of participants in the collision, which depends on the nuclei  $A$  and  $B$ , and the impact parameter.  $N_{AB}^{\text{coll}}$  is the number of binary collisions in the process. We present results for Au+Au and Cu+Cu collisions at RHIC at  $\sqrt{S} = 0.2$  TeV per nucleon pair and Pb+Pb collisions at LHC at  $\sqrt{S} = 2.76$  TeV per nucleon pair.

We emphasize up front that our goal is not to fit data in heavy ion reactions but to investigate systematically the relative significance of CNM and QGP effects and discuss ways in which these effects can be better constrained. Our formalism is limited to high transverse momentum and not applicable to  $p_T$ -integrated yields. The CNM [18] effects we consider include nuclear shadowing (here implemented as coherent power corrections) and initial state energy loss. These are calculated in the same framework as previously used for light hadrons [19–26] and open heavy flavor [27–29]. We also consider transverse momentum broadening [19, 28–30] (as a model for the Cronin effect). We give results for the p(d)+A collisions at RHIC and the LHC with and without considering the Cronin effect. Since the CNM effects are generated on a short time scale,  $\sim (1\text{fm}/c)A^{1/3}/\gamma$  (where  $A$  is the atomic mass number of the nucleus and  $\gamma = 1/\sqrt{1-v^2}$  is the Lorentz factor, and  $A^{1/3}/\gamma$  is roughly the Lorentz contracted size of the nucleus in the lab frame in fm), compared to the formation time of the quarkonia, we take the  $Q\bar{Q}$  pair in the final state in the CNM calculation as the “proto-quarkonium” state.

We include two effects of  $Q\bar{Q}$  propagation through the thermal medium. First, on time scales shorter than the formation time of quarkonia, the color-octet component of the proto-quarkonium state will be quenched. This effect is included by calculating the quenching factor for a massive color-octet state passing through the medium for the formation time. Second, on time scales longer than the formation time, the quarkonia can be dissociated by the medium. We include this by solving the rate equations [31, 32] describing the change in the yields of quarkonia as a function of time. The microscopic input for the equations are the time scales for the formation and the dissociation of the quarkonia. Since the size of proto-quarkonium is small, it is typically assumed that the formation time  $t_{\text{form}}$  for the “proto-quarkonium” to “expand” into the quarkonium wavefunction, is not significantly modified by the presence of the QGP [9]. Hence,  $t_{\text{form}}$  in the rest frame of the meson is  $\sim 1/(m_Q v^2)$ . We estimate  $t_{\text{form}}$  by dividing the radial size of the wavefunction by the radial velocity and assign a factor of 2 uncertainty to it. (Some equilibrium approaches [6] include effects of a finite time of formation by suppressing the decay rate.)

For dissociation times, most studies use results for thermally equilibrated quarkonia [6, 8, 9]. For a quarkonium which is stationary or slowly moving through the thermal medium it might be safe to assume that it reaches thermal equilibrium with the medium. In this picture, the wavefunction of the quarkonium (the lowest Fock component) is better described by the solution of the Schrödinger equation with a modified potential that depends on the temperature [2, 8–10]. The potentials used are based on finite temperature lattice calculations of the potential between two static charges [33]. The dissociation rates have been calculated in several approaches. In [34, 35] the imaginary part of the potentials — which is related to dissociation — has been calculated in the hard thermal loop framework. In [36] the thermal width has been calculated using the calculation of collisional decay rates [37]. In [8] a  $T$ -matrix approach was used to calculate decay rates of thermal states. For a review of thermal properties of quarkonia using AdS/CFT techniques see [38].

If a quarkonium state is produced on a short formation time scale and is moving rapidly through the QGP, it may not have sufficient time to thermally equilibrate with the medium. As it propagates through the hot and dense matter, collisions with thermal gluons can dissociate the quarkonium on a time scale  $t_{\text{diss}}$  [31, 32, 39, 40]. In this paper, we take this high- $p_T$  limit and explore the consequence of assuming that the wavefunction of the meson is the same as in the vacuum, and that the main impact of the medium is to dissociate the meson as it propagates through it. This dissociation mechanism has been phenomenologically successful in describing the modification of the yields of open heavy flavor mesons as a function of the transverse momentum  $p_T$ . At RHIC, this mechanism is consistent with the large suppression of non-photonic electrons [41–43]. The predictions [32] for  $D$ -meson suppression at the LHC are

compatible with preliminary experimental results [44]. The formation times for quarkonia are also small. Therefore, in-medium formation and dissociation can modify the quarkonia yields. Before the formation of the quarkonium state, the production of  $Q\bar{Q}$  in the color-octet state is the dominant mechanism for quarkonia production. As mentioned above this colored object loses energy, which quenches the yield of quarkonia. After formation, an overall color neutral object with a dominant color-singlet wavefunction propagates through the medium and is dominantly lost via dissociation. We find the dissociation time  $t_{\text{diss}}$  for the color-singlet Fock component of the quarkonium wavefunction by calculating the rate of broadening of the wavefunction due to in-medium interactions, as described for open heavy flavor in [31]. One important difference with the heavy-light mesons is that the probability of reformation after dissociation is small since the probability of refragmentation to quarkonia is small. In principle, recombination [45] with thermal  $\bar{Q}$  and  $Q$  from the medium can re-generate quarkonia. Since the population of thermal heavy quarks is exponentially suppressed ( $\sim e^{-m_T/T}$ ), especially at large  $p_T$ , we ignore this process.

Our results for the  $R_{AA}$  of  $J/\psi$  mesons, obtained using this formalism, are consistent with PHENIX and STAR data for central Au+Au and Cu+Cu collisions. p+A quarkonium yields at high  $p_T$  are necessary to accurately constrain the magnitude of CNM effects. Results from ATLAS and CMS at the LHC for the  $J/\psi$  suppression are well reproduced by the calculation only in peripheral and mid-central collisions. It is difficult (with or without transverse momentum broadening) to obtain a five-fold suppression of prompt  $J/\psi$ , as reported by the CMS experiment at the LHC, without assuming thermal effects at the level of the quarkonium wavefunction. For the  $\Upsilon$ s, this approach predicts that the suppression for the  $\Upsilon(2S)$  and  $\Upsilon(3S)$  at high  $p_T$  is comparable to the  $\Upsilon(1S)$  suppression. (This statement is true for the direct production of  $\Upsilon(1S)$  and  $\Upsilon(2S)$ . The feed-down contributions to  $\Upsilon(1S)$ ,  $\Upsilon(2S)$ , and  $\Upsilon(3S)$  from the  $p$ -wave states are suppressed differently, but we find their  $R_{AA}$  to be comparable even when we include feed-down from  $p$ -wave states.) This prediction is also different from the expectation of the equilibrium models, which predict stronger suppression (smaller  $R_{AA}$ ) for the excited states. Differential high transverse momentum data is also necessary to shed light on the possible thermal modification of boosted  $\Upsilon$ s at the LHC.

Our paper is organized as follows. In Section II we present the calculation of the p+p baseline yields of quarkonia. In Section III we discuss how CNM effects modify the production yields of quarkonia in nuclear collisions. In Section IV we evaluate the wavefunctions needed for the evaluation of the formation and dissociation time scales. In Section V we calculate the dissociation time scale in the QGP and discuss the dynamics of quarkonia as they propagate through the strongly-interacting medium. Results for the nuclear modification factor in p+A and A+A collisions are given in Section VI. We present our conclusions in Section VII. We discuss the details of fitting the color-octet matrix elements for  $J/\psi$  ( $\Upsilon$ ) production in Appendix A (Appendix B). The contribution of feed-down from  $B$ -decay is given in Appendix C and results for  $R_{AA}$  at forward rapidity at LHC energies is shown in Appendix D.

## II. QUARKONIUM PRODUCTION IN P+P COLLISIONS

In this section we describe the production of quarkonia at high transverse momenta in p+p collisions. This provides a baseline for the calculation of the nuclear modification factor  $R_{AB}(p_T)$  defined above in Eq. 1. It also gives the initial unquenched spectrum of “proto-quarkonia” in the heavy ion collision, excluding CNM effects and effects of the propagation of the quarkonium states through the QGP medium.

The dominant processes in evaluating the differential yields of heavy mesons as a function of  $p_T$  are the  $2 \rightarrow 2$  processes of the kind  $g + q \rightarrow H + q$ ,  $q + \bar{q} \rightarrow H + g$  and  $g + g \rightarrow H + g$ , where  $H$  refers to the heavy meson. We label the process generically as  $a + b \rightarrow c + d$ , where  $a$  and  $b$  are light incident partons,  $c$  refers to  $H$  and  $d$  is a light final-state parton. Given the scattering matrix for the process,  $\mathcal{M}_{ab \rightarrow cd}$ , the cross section has the form

$$\frac{d\sigma}{dp_T dy} = \int dx_a \phi_a(x_a, \mu_F) \phi_b(x_b, \mu_F) \frac{2p_T}{x_a - \frac{m_T}{\sqrt{S}} e^y} x_a x_b \frac{d\sigma}{d\hat{t}}(ab \rightarrow cd), \quad (2)$$

where  $\phi_a$  ( $\phi_b$ ) is the distribution function of parton  $a$  ( $b$ ) in the incident hadron traveling in the  $+z$  ( $-z$ ) direction. (In our calculations we use leading order (LO) 2008 MSTW distribution functions [46].) We denote by  $x_a$  ( $x_b$ ) the fraction of the large light-cone momentum of the hadron carried by the parton. In Eq. 2,  $\sqrt{S}$  is the center-of-mass energy of the incident hadrons. Momentum-energy conservation fixes

$$x_b = \frac{1}{\sqrt{S}} \frac{x_a \sqrt{S} m_T e^{-y} - m_H^2}{x_a \sqrt{S} - m_T e^y}. \quad (3)$$

We take the factorization and renormalization scales  $\mu_F$ ,  $\mu_R$  to be  $m_T = \sqrt{p_T^2 + m_H^2}$ , where  $m_H \sim 2m_Q$  is the meson mass. We will analyze the uncertainty associated with the scale by varying the scale from  $m_T/2$  to  $2m_T$ . The

invariant cross section is given by

$$\frac{d\sigma}{d\hat{t}} = \frac{|\mathcal{M}|^2}{16\pi\hat{s}^2}, \quad (4)$$

where  $\hat{s}$ ,  $\hat{t}$ , and  $\hat{u}$  are the parton level Mandelstam variables.

### A. NRQCD calculation of $d\sigma/d\hat{t}$

We use LO NRQCD [12] results to calculate the production of quarkonia in p+p collisions. NRQCD provides a systematic procedure to compute any quantity as an expansion in the relative velocity  $v$  of the heavy quarks in the meson. For example, the wavefunction of the  $J/\psi$  meson (analogous expressions hold for the  $\psi(2S)$ ,  $\Upsilon(1S)$ ,  $\Upsilon(2S)$  and  $\Upsilon(3S)$ ) is written as

$$\begin{aligned} |J/\psi\rangle = & |Q\bar{Q}([{}^3S_1]_1)\rangle + \mathcal{O}(v)|Q\bar{Q}([{}^1S_0]_{8g})\rangle + \mathcal{O}(v^2)|Q\bar{Q}([{}^3S_1]_{8gg})\rangle \\ & + \mathcal{O}(v^1)|Q\bar{Q}([{}^3P_0]_{8g})\rangle + \mathcal{O}(v^1)|Q\bar{Q}([{}^3P_1]_{8g})\rangle + \mathcal{O}(v^1)|Q\bar{Q}([{}^3P_2]_{8g})\rangle + \dots \end{aligned} \quad (5)$$

The differential cross section for the prompt (as opposed to inclusive, which includes contributions from  $B$ -hadron decay) and direct (as opposed to indirect, from the decay of heavier charmed mesons) production of  $J/\psi$  can also be calculated in NRQCD. It can be written as the sum of the contributions,

$$\begin{aligned} d\sigma(J/\psi) = & d\sigma(Q\bar{Q}([{}^3S_1]_1))\langle\mathcal{O}(Q\bar{Q}([{}^3S_1]_1) \rightarrow J/\psi)\rangle + d\sigma(Q\bar{Q}([{}^1S_0]_8))\langle\mathcal{O}(Q\bar{Q}([{}^1S_0]_8) \rightarrow J/\psi)\rangle \\ & + d\sigma(Q\bar{Q}([{}^3S_1]_8))\langle\mathcal{O}(Q\bar{Q}([{}^3S_1]_8) \rightarrow J/\psi)\rangle + d\sigma(Q\bar{Q}([{}^3P_0]_8))\langle\mathcal{O}(Q\bar{Q}([{}^3P_0]_8) \rightarrow J/\psi)\rangle \\ & + d\sigma(Q\bar{Q}([{}^3P_1]_8))\langle\mathcal{O}(Q\bar{Q}([{}^3P_1]_8) \rightarrow J/\psi)\rangle + d\sigma(Q\bar{Q}([{}^3P_2]_8))\langle\mathcal{O}(Q\bar{Q}([{}^3P_2]_8) \rightarrow J/\psi)\rangle + \dots, \end{aligned} \quad (6)$$

where the quantity in the brackets  $[ ]$  represents the angular momentum quantum numbers of the  $Q\bar{Q}$  pair in the Fock expansion. The subscript on  $[ ]$  refers to the color structure of the  $Q\bar{Q}$  pair, 1 being the color-singlet and 8 being the color-octet. The dots represent terms which contribute at higher powers of  $v$ . The short distance cross sections  $d\sigma(Q\bar{Q})$  correspond to the production of a  $Q\bar{Q}$  pair in a particular color and spin configuration, while the long distance matrix element  $\langle\mathcal{O}(Q\bar{Q}) \rightarrow J/\psi\rangle$  corresponds to the probability of the  $Q\bar{Q}$  state to convert to the quarkonium wavefunction. This probability includes any necessary prompt emission of soft gluons to prepare a color neutral system that matches onto the corresponding Fock component of the quarkonium wavefunction.

Power counting rules tell us that contributions from the color-octet matrix elements in Eq. 6 are suppressed by  $v^4$  compared to the color singlet matrix elements. More specifically,

$$\begin{aligned} \langle\mathcal{O}(Q\bar{Q}([{}^3S_1]_1) \rightarrow J/\psi)\rangle &= \mathcal{O}(m_Q^3 v^3), \\ \langle\mathcal{O}(Q\bar{Q}([{}^3S_1]_8) \rightarrow J/\psi)\rangle &= \mathcal{O}(m_Q^3 v^7), \\ \langle\mathcal{O}(Q\bar{Q}([{}^1S_0]_8) \rightarrow J/\psi)\rangle &= \mathcal{O}(m_Q^3 v^7), \\ \langle\mathcal{O}(Q\bar{Q}([{}^3P_J]_8) \rightarrow J/\psi)\rangle &= \mathcal{O}(m_Q^5 v^7). \end{aligned} \quad (7)$$

These operators are multiplied by the short distance differential cross sections, which are related to the probability to create  $Q\bar{Q}$  pairs in specific quantum states. Since these are short distance operators, they can be calculated in perturbation theory. We use the expressions for the short distance color-singlet cross sections given in [47, 48] and the color-octet cross sections given in [13–15].

The case of the  $p$ -wave bound states ( $\chi_{c0}$ ,  $\chi_{c1}$ , and  $\chi_{c2}$ , sometimes collectively referred to as  $\chi_{cJ}$ , and the corresponding states of the  $b$  quark) is slightly different. The wavefunction of  $\chi_c$  states can be written as

$$\begin{aligned} |\chi_{cJ}\rangle = & |Q\bar{Q}([{}^3P_J]_1)\rangle + \mathcal{O}(v)|Q\bar{Q}([{}^3S_1]_{8g})\rangle + \mathcal{O}(v^2)|Q\bar{Q}([{}^1S_0]_{8g})\rangle + \mathcal{O}(v)|Q\bar{Q}([{}^3D_J]_{8g})\rangle \\ & + \mathcal{O}(v^2)|Q\bar{Q}([{}^1P_1]_{8g})\rangle + \mathcal{O}(v^2)|Q\bar{Q}([{}^3P_J]_{8gg})\rangle + \dots \end{aligned} \quad (8)$$

The color-singlet state  $Q\bar{Q}([{}^3P_J]_1)$  and the color-octet state  $Q\bar{Q}([{}^3S_1]_8)$  contribute to the same order in  $v$  because of the angular momentum barrier for  $p$ -wave states, and hence both need to be included for a consistent calculation in  $v$ . For the calculation of the production cross section, we consistently take the contributions to the lowest order in  $v$ . For example the  $\chi_c$  contribution is

$$d\sigma(\chi_{cJ}) = d\sigma(Q\bar{Q}([{}^3P_J]_1))\langle\mathcal{O}(Q\bar{Q}([{}^3P_J]_1) \rightarrow \chi_{cJ})\rangle + d\sigma(Q\bar{Q}([{}^3S_1]_8))\langle\mathcal{O}(Q\bar{Q}([{}^3S_1]_8) \rightarrow \chi_{cJ})\rangle + \dots \quad (9)$$

Similar expressions hold for the  $\chi_b(1P)$ ,  $\chi_b(2P)$  and  $\chi_b(3P)$  mesons. The expressions for the short distance coefficients are given in [14]. The scaling of the matrix elements is given as

$$\begin{aligned}\langle \mathcal{O}(Q\bar{Q}([{}^3P_J]_1) \rightarrow \chi_{cJ}) \rangle &= \mathcal{O}(m_Q^5 v^5), \\ \langle \mathcal{O}(Q\bar{Q}([{}^3S_1]_8) \rightarrow \chi_{cJ}) \rangle &= \mathcal{O}(m_Q^5 v^5).\end{aligned}\quad (10)$$

Therefore we need the color-singlet and color-octet matrix elements to obtain theoretical results for the production of quarkonia at RHIC for  $\sqrt{S} = 0.2$  TeV and at the LHC for  $\sqrt{S} = 2.76$  TeV. We estimate the matrix elements by fitting to yields obtained at the TeVatron, RHIC, and at the LHC.

## B. Feed-down contributions

In this paper we will focus on the  $p_T$  differential yields of  $J/\psi$ ,  $\Upsilon(1S)$ ,  $\Upsilon(2S)$ , and  $\Upsilon(3S)$  mesons. Section II A gives expressions for the direct production cross sections of these and for the  $p$ -wave quarkonia. Excited states of the mesons decay to the states of lower energy on a short time scale and therefore we include these feed-down contributions to obtain what is called the prompt yield.

For example,  $\chi_{cJ}$  and  $\psi(2S)$  contribute to the prompt yields of  $J/\psi$ . Therefore we need the color-singlet and color-octet matrix elements for each of these species, which we give in Section II C. (Details about the fitting procedure to obtain the color-octet matrix elements and the feed-down contributions to prompt  $J/\psi$  are discussed in Appendix A.)

$B$  hadrons can also decay to  $J/\psi$  with a net effective branching fraction  $B(H_b \rightarrow J/\psi + X)_{\text{eff}} = 1.16 \times 10^{-2}$  [50]. In particular, at high  $p_T$ , the contribution to the inclusive yield from the decay of  $B$ -hadrons is substantial, and can possibly even dominate production. At the LHC and the TeVatron the  $B$ -decay contributions have been separately measured [50, 54], while RHIC [55, 56] reports the inclusive yields. In Fig. 1 in Section II D we will only show the prompt production yields and discuss the  $B$  feed-down contribution in Appendix C.

Similarly, for  $\Upsilon(1S)$  production, we consider states up to  $\Upsilon(3S)$ . The relevant color-singlet and -octet matrix elements are given in Section II C. (Details about the fitting procedure and the feed-down contributions to prompt  $\Upsilon(1S)$  are discussed in Appendix B.)

## C. Matrix elements for quarkonia production

In this work, following [13, 14] we use the values of the color-singlet operators calculated using the potential model. The expressions and the values for the color-singlet operators are given in [13, 14, 49]. The values are obtained by solving the non-relativistic wavefunctions:

$$\begin{aligned}\langle \mathcal{O}(c\bar{c}([{}^3S_1]_1) \rightarrow J/\psi) \rangle &= 3\langle \mathcal{O}(c\bar{c}([{}^1S_0]_1) \rightarrow J/\psi) \rangle &= 3N_c \frac{|R_{n=1}(0)|^2}{2\pi} &= 1.2 \text{ GeV}^3, \\ \langle \mathcal{O}(c\bar{c}([{}^3S_1]_1) \rightarrow \psi(2S)) \rangle &= 3\langle \mathcal{O}(c\bar{c}([{}^1S_0]_1) \rightarrow \psi(2S)) \rangle &= 3N_c \frac{|R_{n=2}(0)|^2}{2\pi} &= 0.76 \text{ GeV}^3, \\ \frac{1}{5}\langle \mathcal{O}(c\bar{c}([{}^3P_2]_1) \rightarrow \chi_{c2}(1P)) \rangle &= \frac{1}{3}\langle \mathcal{O}(c\bar{c}([{}^3P_1]_1) \rightarrow \chi_{c1}(1P)) \rangle = \\ &\langle \mathcal{O}(c\bar{c}([{}^3P_0]_1) \rightarrow \chi_{c0}(1P)) \rangle &= 3N_c \frac{|R'_{n=1}(0)|^2}{2\pi} &= 0.054 m_{\text{charm}}^2 \text{ GeV}^3,\end{aligned}\quad (11)$$

where  $R(0)$  is the radial wavefunction at the origin,  $R'(0)$  is the first derivative of the radial wavefunction at the origin, and  $n$  refers to the radial quantum number. We take the mass of the charm quark,  $m_{\text{charm}} = 1.4 \text{ GeV}$  [16].

The values of the color-singlet operators for bottomonia are given in [15], which we reproduce here:

$$\begin{aligned}\langle \mathcal{O}(b\bar{b}([{}^3S_1]_1) \rightarrow \Upsilon(1S)) \rangle &= 3N_c \frac{|R_{n=1}(0)|^2}{2\pi} &= 10.9 \text{ GeV}^3, \\ \langle \mathcal{O}(b\bar{b}([{}^3P_0]_1) \rightarrow \chi_{b0}(1P)) \rangle &= 3N_c \frac{|R'_{n=1}(0)|^2}{2\pi} &= 0.100 m_{\text{bottom}}^2 \text{ GeV}^3, \\ \langle \mathcal{O}(b\bar{b}([{}^3S_1]_1) \rightarrow \Upsilon(2S)) \rangle &= 3N_c \frac{|R_{n=2}(0)|^2}{2\pi} &= 4.5 \text{ GeV}^3, \\ \langle \mathcal{O}(b\bar{b}([{}^3P_0]_1) \rightarrow \chi_{b0}(2P)) \rangle &= 3N_c \frac{|R'_{n=2}(0)|^2}{2\pi} &= 0.036 m_{\text{bottom}}^2 \text{ GeV}^3, \\ \langle \mathcal{O}(b\bar{b}([{}^3S_1]_1) \rightarrow \Upsilon(3S)) \rangle &= 3N_c \frac{|R_{n=3}(0)|^2}{2\pi} &= 4.3 \text{ GeV}^3,\end{aligned}\quad (12)$$

where we use  $m_{\text{bottom}} = 4.88 \text{ GeV}$  [13, 14].

The color-octet operators can not be related to the non-relativistic wavefunctions of  $Q\bar{Q}$  since it involves a higher Fock state. Following [13–15], we fit them to the data.

For the charm mesons we use data from the TeVatron [50, 52, 53, 61], RHIC [55, 56], and the LHC [54, 62] (see Fig. 1, and Appendix A for details). We obtain the following values:

$$\begin{aligned}
\langle \mathcal{O}(c\bar{c}([{}^3S_1]_8) \rightarrow J/\psi) \rangle &= (0.0013 \pm 0.0013) \text{ GeV}^3, \\
\langle \mathcal{O}(c\bar{c}([{}^1S_0]_8) \rightarrow J/\psi) \rangle &= (0.018 \pm 0.0087) \text{ GeV}^3, \\
&= \langle \mathcal{O}(c\bar{c}([{}^3P_0]_8) \rightarrow J/\psi) \rangle / (m_{\text{charm}}^2), \\
\langle \mathcal{O}(c\bar{c}([{}^3S_1]_8) \rightarrow \psi(2S)) \rangle &= (0.0033 \pm 0.00021) \text{ GeV}^3, \\
\langle \mathcal{O}(c\bar{c}([{}^1S_0]_8) \rightarrow \psi(2S)) \rangle &= (0.0080 \pm 0.00067) \text{ GeV}^3, \\
&= \langle \mathcal{O}(c\bar{c}([{}^3P_0]_8) \rightarrow J/\psi) \rangle / (m_{\text{charm}}^2), \\
\langle \mathcal{O}(c\bar{c}([{}^3P_1]_8) \rightarrow J/\psi) \rangle &= 3 \times \langle \mathcal{O}(c\bar{c}([{}^3P_0]_8) \rightarrow J/\psi) \rangle, \\
\langle \mathcal{O}(c\bar{c}([{}^3P_2]_8) \rightarrow J/\psi) \rangle &= 5 \times \langle \mathcal{O}(c\bar{c}([{}^3P_0]_8) \rightarrow J/\psi) \rangle, \\
\langle \mathcal{O}(c\bar{c}([{}^3S_1]_8) \rightarrow \chi_{c0}(1P)) \rangle &= (0.00187 \pm 0.00025) \text{ GeV}^3,
\end{aligned} \tag{13}$$

Since the shape of the short distance part as a function of  $p_T$  is very similar for  $[{}^1S_0]_8$  and  $[{}^3P_0]_8$  contributions [13, 14], we do not attempt to fit the two long distance matrix elements separately and only fit a linear combination. The  $\chi^2/\text{dof} = 4.56$  for the  $\chi_{cJ}$  feed-down contribution,  $\chi^2/\text{dof} = 5.6$  for the  $\psi(2S)$  contribution, and  $\chi^2/\text{dof} = 5.2$  for the  $J/\psi$  direct production.

The octet matrix elements for the bottomonia are obtained by fitting TeVatron [51] and the LHC [60] (see Fig. 2, and Appendix B for details) data and are as follows:

$$\begin{aligned}
\langle \mathcal{O}(b\bar{b}([{}^3S_1]_8) \rightarrow \Upsilon(1S)) \rangle &= (0.0477 \pm 0.0334) \text{ GeV}^3, \\
\langle \mathcal{O}(b\bar{b}([{}^1S_0]_8) \rightarrow \Upsilon(1S)) \rangle &= (0.0121 \pm 0.040) \text{ GeV}^3, \\
&= \langle \mathcal{O}(b\bar{b}([{}^3P_0]_8) \rightarrow \Upsilon(1S)) \rangle / (5m_{\text{bottom}}^2), \\
\langle \mathcal{O}(b\bar{b}([{}^3S_1]_8) \rightarrow \chi_{b0}(1P)) \rangle &= (0.1008) \text{ GeV}^3, \\
\langle \mathcal{O}(b\bar{b}([{}^3S_1]_8) \rightarrow \Upsilon(2S)) \rangle &= (0.0224 \pm 0.02) \text{ GeV}^3, \\
\langle \mathcal{O}(b\bar{b}([{}^1S_0]_8) \rightarrow \Upsilon(2S)) \rangle &= (-0.0067 \pm 0.0084) \text{ GeV}^3, \\
&= \langle \mathcal{O}(b\bar{b}([{}^3P_0]_8) \rightarrow \Upsilon(2S)) \rangle / (5m_{\text{bottom}}^2), \\
\langle \mathcal{O}(b\bar{b}([{}^3S_1]_8) \rightarrow \chi_{b0}(2P)) \rangle &= (0.0324) \text{ GeV}^3, \\
\langle \mathcal{O}(b\bar{b}([{}^3S_1]_8) \rightarrow \Upsilon(3S)) \rangle &= (0.0513 \pm 0.0085) \text{ GeV}^3, \\
\langle \mathcal{O}(b\bar{b}([{}^1S_0]_8) \rightarrow \Upsilon(3S)) \rangle &= (0.0002 \pm 0.0062) \text{ GeV}^3, \\
&= \langle \mathcal{O}(b\bar{b}([{}^3P_0]_8) \rightarrow \Upsilon(3S)) \rangle / (5m_{\text{bottom}}^2)
\end{aligned} \tag{14}$$

The  $\chi^2/\text{dof} = 1.3$  for  $\Upsilon(3S)$ , 3.5 for  $\Upsilon(2S)$  and 3.8 for  $\Upsilon(1S)$ .

For a more sophisticated fitting of the color-octet matrix elements including NLO effects, see [57–59]. The matrix elements including feed-down effects obtained in [59] are similar, albeit slightly smaller than our estimates.

#### D. Quarkonia yields in p+p and p+p̄ collisions

Shown in Fig. 1 are yields for  $J/\psi$  production at the TeVatron, RHIC and the LHC at  $\sqrt{S} = 1.96, 0.2,$  and 7 TeV, respectively. The data from CDF [50] at the TeVatron and from ATLAS [54] at the LHC shows the prompt production and can, therefore, directly be compared to the theoretical curves of the prompt yields obtained from NRQCD and shown in Fig. 1. Comparison with prompt production yields measured by CMS [73] at  $\sqrt{S} = 2.76$  TeV is given in Fig. 10 in Appendix A where the feed-down contributions from  $\chi_{cJ}$  and  $\psi(2S)$  are also shown explicitly.

The PHENIX [55] and STAR [56] data from RHIC shows the inclusive yields. The theoretical curve is for the prompt yield. Including the  $B$  feed-down contribution at RHIC energies gives an inclusive yield roughly 20 – 50% larger, slightly improving agreement with PHENIX data. The ratios of the  $B$  feed-down contributions to the prompt yields are shown in Appendix C.

We also show the uncertainty associated with the factorization and renormalization scales  $\mu_R, \mu_F$  by taking  $\mu_R = \mu_F = m_T/2$  (upper curves),  $\mu_r = \mu_F = m_T$  (central curves) and  $\mu_R = \mu_F = 2m_T$  (lower curves). This scale variation

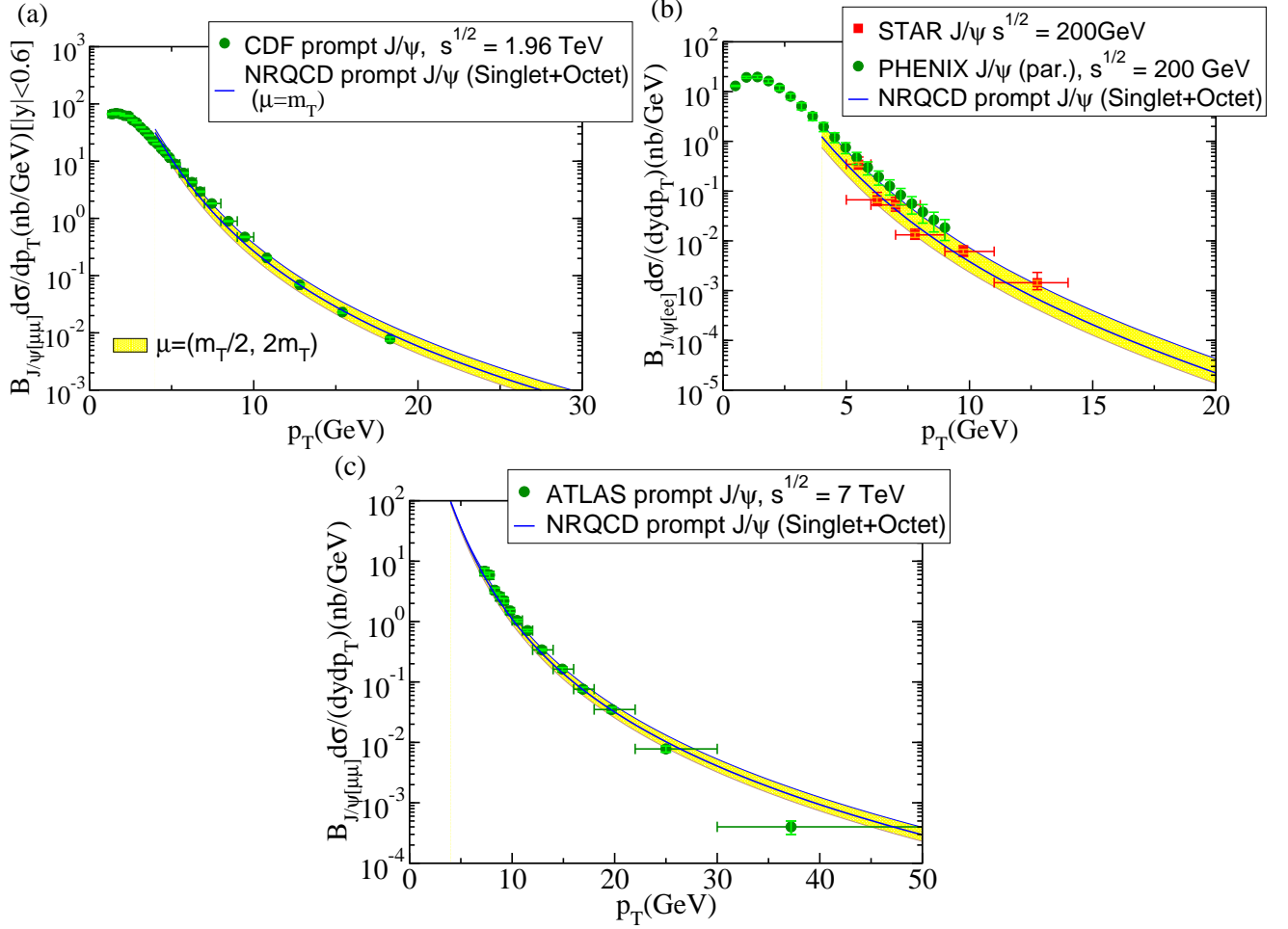


FIG. 1: (Color online)  $J/\psi$  production yields multiplied by the branching ratios,  $B(J/\psi \rightarrow ee) \simeq B(J/\psi \rightarrow \mu\mu) \simeq 5.93\%$ . The upper left panel corresponds to data for the yields of  $J/\psi$  from CDF at  $\sqrt{S} = 1.96$  TeV [50]. The upper right panel is for RHIC at  $\sqrt{S} = 0.2$  TeV with inclusive data from the PHENIX experiment [55] (using the fit given in [55]) and the STAR experiment [56]. The bottom panel has prompt data from the LHC at  $\sqrt{S} = 7$  TeV from the ATLAS collaboration [54] The darker colored error bars (dark green or red) give the systematic errors and the lighter colored give the statistical errors in the experimental data. The solid line (blue) are the theoretically calculated prompt yields. We show the uncertainty associated with changing the renormalization scale with a band (yellow). The upper curves are obtained for  $\mu_R = \mu_F = m_T/2$ , the central for  $\mu_R = \mu_F = m_T$  and the lower for  $\mu_R = \mu_F = 2m_T$ . The CDF results are for rapidity  $|y| < 0.6$ , and the RHIC and LHC results are quoted per unit rapidity at mid rapidity.

affects the cross section in the following two ways (as can be seen in Eq. 2). First, the parton distribution functions at a higher scale for the same value of  $x$  are smaller in the regime of interest. Second, the strong coupling constant  $\alpha_s$  decreases with increasing scale. These effects give a variation in the yields as shown in Fig. 1.

We see that the NRQCD results are a bit less steep than the data. The results for RHIC at  $\sqrt{S} = 0.2$  TeV provide the baseline for the p+p yield, which we use to calculate  $R_{AA}$ . For the LHC, we need the baseline at a center-of-mass energy  $\sqrt{S} = 2.76$  TeV, which is given in Fig. 10 in Appendix A.

The yields of  $b\bar{b}$  states are shown in Fig. 2. For the  $\Upsilon(3S)$  we only consider the direct production and ignore feed-down. For  $\Upsilon(2S)$  we include feed-down from  $\Upsilon(3S)$  and  $\chi_b(2)$ . For  $\Upsilon(1S)$  there is additional feed-down from  $\Upsilon(2S)$  and  $\chi_b(1)$ .

We see that the values of matrix elements that give a good agreement with the LHC data [60] give slightly smaller than measured yields at the Tevatron [51]. We expect that the deviation from the measured yields will be smaller at  $\sqrt{S} = 2.76$  TeV, for which we calculate  $R_{AA}$ . The baseline for this energy is shown in Fig. 11 in Appendix B, where the feed-down contributions are also given.

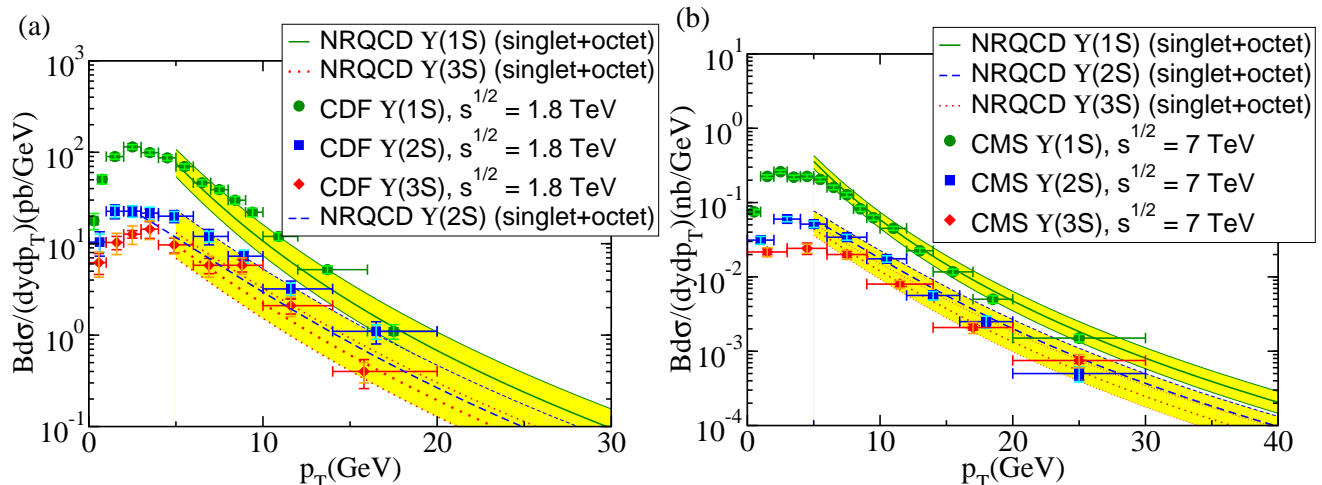


FIG. 2: (Color online)  $\Upsilon$  yields multiplied by the corresponding  $B(\Upsilon \rightarrow \mu\mu)$ . The left panel shows data from the Tevatron at 1.8 TeV [51]. The right panel corresponds to data from CMS at 7 TeV [60]. The solid line (green) is for  $\Upsilon(1S)$ , the dashed (blue) for  $\Upsilon(2S)$  and the dotted (red) for  $\Upsilon(3S)$ . The yellow band shows the uncertainty associated with varying the factorization and the renormalization scale from  $m_T/2$  to  $2m_T$ .

### III. COLD NUCLEAR MATTER EFFECTS

In heavy ion reactions, the production yields of energetic particles are always affected by cold nuclear matter (CNM) effects. These include nuclear shadowing, initial state energy loss and transverse momentum broadening (also interpreted as the origin of the Cronin effect). All these effects are grow linearly with the system size  $L$ , which for CNM effects is proportional to the nuclear size  $R \approx 1.2A^{1/3}$  fm. In our calculation, the CNM effects are calculated from the elastic, inelastic and coherent scattering processes of partons in large nuclei [28].

1. Nuclear shadowing: Shadowing generally refers to the suppression of the inclusive deep-inelastic scattering (DIS) cross section per nucleon in reactions with a nuclear target relative to the corresponding cross section in reactions with a proton target. For Bjorken- $x$  larger than 0.25 (EMC and the Fermi motion regions) the effect is mainly due to collective effects in the nucleus [63]. In this region shadowing can be parametrized as a modification of the parton distribution function  $\phi(x)$  by a factor which depends on  $x$ . We use the EKS98 modification factor provided in [64]. For  $x < 0.1$ , power-suppressed resummed [21, 22] coherent final-state scattering of the struck partons leads to suppression in the observed cross sections. These are included in our calculation and modify the momentum fractions of the incident partons in Eq. 2 as follows [28]:

$$\tilde{x}_a = x_a \left[ 1 + \frac{\xi_d^2 (A^{1/3} - 1)}{-\hat{t} + m_d^2} \right], \quad \tilde{x}_b = x_b \left[ 1 + \frac{\xi_c^2 (A^{1/3} - 1)}{-\hat{u} + m_c^2} \right], \quad (15)$$

where  $x_a, b$  are the Bjorken- $x$  of the colliding partons. In Eqs. 15  $\hat{t}, \hat{u}$  are the relevant Mandelstam variables at the partonic level and  $m_c, m_d$  are the masses of the struck partons labeled as in Eq. 2. In this case we treat the octet  $Q\bar{Q}$  state as a massive gluon with  $m_c = m_H$ . Immediately after the hard scattering the unexpanded color-singlet state does not couple to the medium. (Equivalently, its color factor is 0.) Following previous studies [32], we use  $(\xi_{q,g}^2 A^{1/3}) \approx (2\mu^2 L / \lambda_{q,g})$ , which yields  $(\xi_q^2) \approx 0.12 \text{ GeV}^2$  and  $(\xi_g^2) \approx 0.27 \text{ GeV}^2$ . Here  $\mu^2$  is related to the gluon density in the nucleus [28], and  $\lambda_{q(g)}$  are the quark (gluon) mean free paths respectively. The parameters  $\mu$  and  $\lambda_{q,g}$  also determine the transverse momentum broadening as we shall see below in item 3.

2. Initial state energy loss: Before the large  $Q^2$  parton scattering process, the incoming partons lose radiatively a fraction of their energy due to multiple interactions in the target nucleus. If the colliding partons  $a, b$  lose fractional energy  $\epsilon_{a,b} = \frac{\Delta E_{a,b}}{E_{a,b}}$ , to satisfy the same final-state kinematics they must initially carry a larger fraction of the colliding hadron momentum and, correspondingly, a larger value of  $x$ . This can be implemented in Eq. 2 by the following modification

$$\phi_a(\tilde{x}_a) \rightarrow \tilde{\phi}_a(x_a) = \phi_a \left( \frac{\tilde{x}_a}{1 - \epsilon_a} \right), \quad \phi_b(\tilde{x}_b) \rightarrow \tilde{\phi}_b(x_b) = \phi_b \left( \frac{\tilde{x}_b}{1 - \epsilon_b} \right), \quad \tilde{x}_{a,b} \leq 1, \quad (16)$$

in the parton distribution functions  $\phi_{a,b/N}(\tilde{x}_{a,b}, \mu_F)$ . The medium-induced radiative corrections factorize as a standard integral convolution [65]. If  $P_{q,g}(\epsilon)$  is the probability density for quarks and gluons to lose a fraction  $\epsilon$  of their energy, it can be implemented in the cross section calculation as follows [25]:

$$\int dx \phi_q(x) \cdots \rightarrow \int d\tilde{x} \int d\epsilon \phi_q\left(\frac{\tilde{x}}{1-\epsilon}\right) P_q(\epsilon), \quad \int dx \phi_g(x) \cdots \rightarrow \int d\tilde{x} \int d\epsilon \phi_g\left(\frac{\tilde{x}}{1-\epsilon}\right) P_g(\epsilon). \quad (17)$$

The calculation of  $P(\epsilon)$  is described in [23].

3. Cronin effect: In p+A and A+A reactions, Cronin effect can be modeled at the level of the  $p_T$ -differential cross sections by including the  $k_T$  (transverse momentum) broadening of incoming partons that arises from initial-state scattering [19, 30]. This involves relaxing the assumption that the incident partons  $a, b$  in Eq. 2 are collinear and allowing them to carry a transverse momentum  $k_{T a, b}$  with model distributions  $f(k_{T a, b})$ . The advantage of using a simple normalized Gaussian form for  $f(k_{T a, b})$  is the additive variance property:

$$\langle k_{T a, b}^2 \rangle_{AB} = \langle k_{T a, b}^2 \rangle_{NN} + \langle k_{T a, b}^2 \rangle_{IS}, \quad \langle k_{T a, b}^2 \rangle_{IS} = \left\langle \frac{2\mu^2 L}{\lambda_{q,g}} \right\rangle \xi, \quad (18)$$

where  $\langle k_{T a, b}^2 \rangle_{IS}$  accounts for increased momentum broadening in the initial state (IS) in collisions with nuclei. Specifically, in Eq. 18  $\mu^2 = 0.12 \text{ GeV}^2$  appears also in the calculation of the shadowing, and is also related to the dynamical mass of gluons in the nucleus. It sets the scale for the typical transverse momentum exchanged with the gluons of the incident nucleus.  $\lambda_g = (C_F/C_A)\lambda_q$  is the mean free path of the parton, where  $C_F/C_A = 4/9$  is the ratio of the color Casimir factors in the fundamental and the adjoint representation. We take  $\lambda_g = 1 \text{ fm}$  [19].  $\xi$  is a dimensionless numerical factor that accounts for the enhancement of the broadening coming from the power-law tails of the Moliere multiple scattering [78] and is expected to be greater than 1. Typical values used are  $\xi \sim 2 - 3$  [31]. For light final-state partons, the Cronin effect is well studied phenomenologically [19]. For  $D$ -meson and  $B$ -meson production the Cronin effect was discussed in [32]. We note that a 33% reduction of the logarithmic enhancement factor  $\xi$  relative to the one used in [32] gives a better description of the  $p_T \sim 2 - 10 \text{ GeV}$  light hadron production and this is what we use in our work. For quarkonia, the effect of initial-state transverse momentum broadening is not well understood. To our knowledge, this is the first attempt to calculate the Cronin effect for  $Q\bar{Q}$  production. We do not try to constrain its magnitude phenomenologically and point out that data from p+A reactions is needed to constrain all CNM effects. We find that including transverse momentum broadening in the same way as is done for light final states reduces the suppression for  $p_T$  between 3 and 10 GeV significantly and may actually lead to a small enhancement of the charmonium cross section. It is not clear, given the large error bars, whether the Au+Au and Cu+Cu data at RHIC are better described by the Cronin calculation. In contrast, it is evident that the Cronin effect is not consistent with Pb+Pb data at the LHC, which sees a large attenuation at  $p_T \sim 8 \text{ GeV}$ . In Section VIA we will discuss the yields without the Cronin effect. We will discuss the phenomenology of the Cronin effect in Section VIB.

#### IV. QUARKONIUM WAVEFUNCTIONS

The color-singlet matrix elements are proportional to the square of the value of the  $l^{\text{th}}$  derivative of the radial wavefunction of the  $Q\bar{Q}$  Fock state at the origin, where  $l$  refers to the orbital angular momentum of the bound state. Also, for the calculation of the collisional dissociation rate, it is convenient to use wavefunctions in the light-cone coordinate system. We obtain these by taking the Fourier transformation of the spatial wavefunctions and changing the momentum variables to light-cone coordinates. In this section we describe the calculation of these bound state wavefunctions of the heavy mesons. In the calculations, we will assume that high  $p_T$  quarkonia do not thermalize and, therefore, we will use only the zero temperature wavefunctions.

##### A. The instantaneous wavefunctions

Making the usual separation of the radial and angular parts of the wavefunction,  $\psi(\mathbf{r}) = Y_l^m(\hat{r})R_{nl}(r)$ , the Schrödinger equation for the radial part of the  $Q\bar{Q}$  state can be written as

$$\left[ -\frac{1}{2\mu_{\text{red}}} \frac{\partial^2}{\partial r^2} + \frac{l(l+1)}{2\mu_{\text{red}} r^2} + V(r) \right] rR_{nl}(r) = (E_{nl} - 2m_Q)rR_{nl}(r), \quad (19)$$

where  $\mu_{\text{red}} = \frac{m_Q}{2}$  is the reduced mass,  $l$  is the angular quantum number,  $n$  the radial quantum number and  $E_{nl}$  is the binding energy. ( $n-1$  is the number of non-trivial nodes of  $R_{nl}$ .)  $V(r)$  is the potential between the two heavy quarks, which can be estimated from the lattice. We use the potential described in [2]. The results are compactly written in Table I and Table II, where we approximate the radial wavefunction as  $R_{nl}(r) = N_r r^l \prod_{i=1, n-1} (1 - \frac{r}{r_0^i}) \exp(-r^2/(2a^2))$ , where  $r_0^i$  are the nodes of the wavefunction in radial coordinates.

For the calculation of the dissociation rate, we also require the form of the wavefunction in momentum space,

$$\tilde{\psi}(\mathbf{k}) = \int d^3r \psi(\mathbf{r}) = Y_l^m(\hat{k}) \tilde{R}_{nl}(k). \quad (20)$$

$\tilde{\psi}(\mathbf{k})$  satisfies the normalization condition  $\int \frac{d^3k}{(2\pi)^3} |\tilde{\psi}(\mathbf{k})|^2 = \frac{1}{(2\pi)^3} \int dk k^2 |\tilde{R}_{nl}(k)|^2 = 1$ . The momentum space wavefunctions are readily related to the light cone wavefunction as described in [32]. In order to simplify the calculations of the dissociation rates, we approximate the momentum space wavefunctions by the form  $\tilde{R}_{nl}(k) = N_k k^l \prod_{i=1, n-1} (1 - \frac{k}{k_0^i}) \exp(-k^2/(2b^2))$ , where  $k_0^i$  are the location of the nodes in the momentum space wavefunction. Our results are again presented in Table I and Table II. The color-singlet operators are given by the expressions Eq. 11.

$l$	$n$	$E_{nl}$ (GeV)	$a_{\perp} = \sqrt{\frac{2}{3}\langle r^2 \rangle}$ (GeV $^{-1}$ )	$k^2$ (GeV $^2$ )	$N_r$ (GeV $^{3/2}$ )	$N_k$ (GeV $^{-3/2}$ )	$r_0$ (GeV $^{-1}$ )	$k_0$ (GeV)	Meson
0	1	0.7003	1.829	0.2988	0.6071	58.55			$J/\psi$
0	1	0.0858	2.978	0.1127	0.4020	296.0	2.375	0.5219	$\psi(2S)$
1	1	0.2678	2.216	0.2036	0.1677	141.3	0	0	$\chi_{c0}, \chi_{c1}, \chi_{c2}$

TABLE I: Charmonia wavefunctions.  $l$  refers to the angular momentum of the  $Q\bar{Q}$  state, while  $n$  is the radial quantum number.  $\sqrt{\langle r^2 \rangle}$  is the root mean square radius of the quarkonium state,  $k^2$  is the mean square momentum.  $N_r$  is the normalization factor and  $r_0$  is the set of roots for the radial wavefunction.  $N_k$  and  $k_0$  are corresponding quantities for the momentum space wavefunctions.

$l$	$n$	$E_{nl}$ (GeV)	$a_{\perp} = \sqrt{\frac{2}{3}\langle r^2 \rangle}$ (GeV $^{-1}$ )	$k^2$ (GeV $^2$ )	$N_r$ (GeV $^{3/2}$ )	$N_k$ (GeV $^{-3/2}$ )	$r_0$ (GeV $^{-1}$ )	$k_0$ (GeV)	Meson
0	1	1.122	1.007	0.9854	1.486	23.92			$\Upsilon(1S)$
0	2	0.5783	1.446	0.4784	1.479	103.7	1.304	1.012	$\Upsilon(2S)$
0	3	0.2139	1.768	0.3199	1.813	236.4	1.106, 2.751	0.615, 1.457	$\Upsilon(3S)$
1	1	0.7102	1.309	0.5832	0.6251	37.9	0	0	$\chi_{b0,1,2}(1P)$
1	2	0.325	1.588	0.3967	1.004	196.9	0, 2.122	0, 1.105	$\chi_{b0,1,2}(2P)$
1	3	0.05109	2.14	0.2183	0.5635	758.4	0, 1.814, 3.621	0, 0.694, 1.453	$\chi_{b0,1,2}(3P)$

TABLE II: Bottomonia wavefunctions. The notation is the same as Table I.

Note that, as mentioned earlier, the  $Q\bar{Q}$  pair produced in the hard collision in a color-octet state has to emit soft gluons to overlap with the wavefunction of the color neutral quarkonium. Eventually, all the components of the  $Q\bar{Q}$  pair give rise to a color neutral quarkonium state, with a hierarchy of contributions given in Eq. 5. We will assume that after formation, the dynamics of the quarkonium are dominated by the color singlet component. To our knowledge exact solutions for the  $n \geq 3$  Fock components of mesons do not exist.

## B. The light-cone wavefunction

Simulations of high- $p_T$  quarkonium dissociation in the QGP require knowledge of the light-cone wavefunctions of the state, which can be represented as follows [31, 32]:

$$|\vec{P}^+; J\rangle = a_n^\dagger(\vec{P}^+; J)|0\rangle = \sum_{n=2(3)}^{\infty} \int \prod_{i=1}^n \frac{d^2\mathbf{k}_i}{\sqrt{(2\pi)^3}} \frac{dx_i}{\sqrt{2x_i}} \times \psi(x_i, \mathbf{k}_i; \{\nu_i\}) \delta\left(\sum_{j=1}^n x_j - 1\right) \delta^2\left(\sum_{j=1}^n \mathbf{k}_j\right) \\ \times |\cdots a_{q_i}^\dagger(x_{q_i} \vec{P}^+ + \mathbf{k}_{q_i}, \nu_{q_i}) \cdots b_{\bar{q}_j}^\dagger(x_{\bar{q}_j} \vec{P}^+ + \mathbf{k}_{\bar{q}_j}, \nu_{\bar{q}_j}) \cdots \cdots c_{g_k}^\dagger(x_{g_k} \vec{P}^+ + \mathbf{k}_{g_k}, \nu_{g_k}) \cdots\rangle. \quad (21)$$

Here,  $\vec{P}^+ \equiv (P^+, \mathbf{P})$  are the large light-cone momentum and transverse momentum components of the hadron, and the momenta of the partons are given by  $(x_i P^+, x_i \mathbf{P} + \mathbf{k}_i)$ . In Eq. 21  $\nu_{q_i}$  is a set of additional relevant quantum

numbers, such as helicity and color. From the normalization of the meson state of fixed projection  $\lambda$  of the total angular momentum  $J$ :

$$\langle \vec{P}^+; J | \vec{P}^+; J \rangle = 2P^+ (2\pi)^3 \delta(P^+ - P'^+) \delta^2(\mathbf{P} - \mathbf{P}') \delta_{\lambda\lambda'} , \quad (22)$$

an integral constraint on the norm of the light-cone wavefunctions  $\psi(x_i, \mathbf{k}_i; \{\nu_i\})$  can be derived.

In the context of Eq. 21, the color-singlet contribution to quarkonium production can be understood as one that is the dominant, lowest order ( $n = 2$ ), Fock component in the hard scattering. A color-octet contribution requires the emission of at least one gluon for a color neutral hadron to be produced. In either case the hadron state can be approximated as:

$$|\vec{P}^+\rangle = \int \frac{d^2\mathbf{k}}{(2\pi)^3} \frac{dx}{2\sqrt{x(1-x)}} \frac{\delta_{c_1 c_2}}{\sqrt{3}} \psi(x, \mathbf{k}) a_Q^\dagger c_1(x\vec{P}^+ + \mathbf{k}) b_Q^\dagger c_2((1-x)\vec{P}^+ - \mathbf{k}) |0\rangle , \quad (23)$$

where, for the color-octet states,  $a^\dagger$  ( $b^\dagger$ ) represent an ‘‘effective’’ heavy quark (anti-quark) in the 3 ( $\bar{3}$ ) state and [32]

$$\psi(x, \mathbf{k}) = \text{Norm} \times \exp\left(-\frac{\mathbf{k}^2 + m_Q^2}{2\Lambda^2 x(1-x)}\right) , \quad \frac{1}{2(2\pi)^3} \int dx d^2\mathbf{k} |\psi(x, \mathbf{k})|^2 = 1 . \quad (24)$$

The light cone wavefunction  $\psi(x, \mathbf{k})$  is obtained from the instantaneous wavefunction  $\psi(r)$  by taking the Fourier transform and changing the longitudinal component of the  $\mathbf{k}$  vector to the light cone coordinates. Details of this change of variables are given in [32], and here we have used the fact that for quarkonia the masses of the constituent quarks are equal and  $(1-x)m_Q + xm_{\bar{Q}} = m_Q$ .

If we introduce the notation  $\Delta\mathbf{k} = \mathbf{k}_1 - \mathbf{k}_2 = 2\mathbf{k}$ , the transverse width  $\Lambda$  of the light-cone wavefunction  $\psi(x, \mathbf{k})$  is determined from the condition:

$$\frac{1}{2(2\pi)^3} \int dx d^2\mathbf{k} \Delta\mathbf{k}^2 |\psi(x, \mathbf{k})|^2 = 4\langle \mathbf{k}^2 \rangle = \frac{2}{3}\kappa^2 . \quad (25)$$

The factor 2/3 comes from the 2D projection of the mean squared transverse momentum  $\kappa^2$  from the instantaneous wavefunction form calculated in Tables I, II.

## V. QUARKONIUM DYNAMICS AT HIGH TRANSVERSE MOMENTUM

In this section we present details of how we treat the propagation of quarkonia through the QGP. There are two important ways in which the medium affects the yields of quarkonia.

First, on time scales shorter than the formation time of the quarkonia, the color-octet component of the proto-quarkonium state undergoes energy loss as it passes through the QGP. Second, on time scales longer than the formation times of the heavy mesons, the meson can undergo dissociation due to collisions with gluons in the thermal medium. The essence of the dissociation model for heavy mesons is that they have short formation times and can therefore form in the medium on a time scale  $t_{\text{form}}$ . Interactions with the thermal medium can dissociate the mesons on a time scale  $t_{\text{diss}}$ . The final yields are determined by rate equations which take into account the formation and dissociation processes. In the next section we first discuss the rate equations abstractly, using  $t_{\text{form}}$  and  $t_{\text{diss}}$  as parameters. In the later sections we will estimate  $t_{\text{form}}$  and calculate  $t_{\text{diss}}$ . For more details on the dissociation model and its application to the phenomenology of open heavy flavor, see [32].

### A. The rate equations

Let us denote by  $N_{Q\bar{Q}}^{\text{hard}}(p_T, \nu)$  the number of perturbatively produced point-like  $Q\bar{Q}$  states at transverse momentum  $p_T$ . Up to an overall multiplicative Glauber scaling factor  $T_{AB}$ ,  $N_{Q\bar{Q}}^{\text{hard}}(p_T, \nu)$  ( $\nu$  represent the quantum numbers of the  $Q\bar{Q}$  state) are linearly related to the cross sections discussed in Section II. The time scale for the hard QCD process is given by  $t \simeq 1/m_T$ , where  $m_T = \sqrt{p_T^2 + m_H^2}$ . For transverse momenta above a few GeV and  $m_{c\bar{c}} > 3$  GeV,  $m_{b\bar{b}} > 9$  GeV, respectively, this production time is very short. Thus, we take this time to be the starting point for the evolution of the  $Q\bar{Q}$  state. The rate of formation of the corresponding hadronic state is given by the inverse formation time  $1/t_{\text{form}}(p_T)$ . In the presence of a medium, the meson multiplicity, which we denote by  $N_{Q\bar{Q}}^{\text{meson}}(p_T, \nu)$ , is reduced by collisional dissociation processes at a rate  $1/t_{\text{diss}}(p_T)$ . Finally, the number of dissociated  $Q\bar{Q}$  pairs with

a net transverse momentum  $p_T$  is  $N_{Q\bar{Q}}^{\text{diss.}}(p_T, \nu)$ . At the transverse momenta that we consider, the probability for the heavy quark  $Q$  or antiquark  $\bar{Q}$  to pick up a thermal partner and reform a quarkonium state is negligible. The heavy (anti)quark fragmentation contribution to quarkonia is also negligible. Heavy quarks fragment primarily into open heavy flavor mesons.

The dynamics of such a system is governed by the following set of ordinary differential equations:

$$\frac{d N_{Q\bar{Q}}^{\text{hard}}(t; p_T, \nu)}{dt} = -\frac{1}{t_{\text{form}}(t; p_T)} N_{Q\bar{Q}}^{\text{hard}}(t; p_T, \nu), \quad (26)$$

$$\frac{d N_{Q\bar{Q}}^{\text{meson}}(t; p_T)}{dt} = \frac{1}{t_{\text{form}}(t; p_T)} N_{Q\bar{Q}}^{\text{hard}}(t; p_T, \nu) - \frac{1}{t_{\text{diss.}}(t; p_T)} N_{Q\bar{Q}}^{\text{meson}}(t; p_T, \nu), \quad (27)$$

$$\frac{d N_{Q\bar{Q}}^{\text{diss.}}(t; p_T, \nu)}{dt} = \frac{1}{t_{\text{diss.}}(t; p_T)} N_{Q\bar{Q}}^{\text{meson}}(t; p_T, \nu), \quad (28)$$

subject to the constraint  $N_{Q\bar{Q}}^{\text{hard}}(t; p_T, \nu) + N_{Q\bar{Q}}^{\text{meson}}(t; p_T, \nu) + N_{Q\bar{Q}}^{\text{diss.}}(t; p_T, \nu) = N_{Q\bar{Q}}^{\text{hard}}(p_T, \nu)$ , and is uniquely determined by the initial conditions

$$N_{Q\bar{Q}}^{\text{hard}}(t = 0; p_T, \nu) = N_{Q\bar{Q}}^{\text{hard}}(\text{quenched}; p_T, \nu), \quad (29)$$

$$N_{Q\bar{Q}}^{\text{meson}}(t = 0; p_T, \nu) = 0, \quad (30)$$

$$N_{Q\bar{Q}}^{\text{diss.}}(t = 0; p_T, \nu) = 0. \quad (31)$$

An important point to note here is that we have incorporated the quenching of the color-octet proto-quarkonium state by using the quenched value of the distributions  $N_{Q\bar{Q}}^{\text{hard}}(\text{quenched}; p_T, \nu)$  as the initial state to the rate equations. In Section VD we will describe how the quenched distributions are obtained. Finally, we note that in Eqs. 28 the evolution of the dissociated  $Q\bar{Q}$  pair into  $D$ - or  $B$ - mesons is not shown since it does not couple back to Eqs. 26, 27.

Realistic simulations include the velocity dependence of the formation rate of all quarkonium states and the velocity, time, and position dependence of their dissociation rate. (We do not write the meson dependence of  $t_{\text{form}}$  and  $t_{\text{diss}}$  to avoid cluttered notation.) It is, however, useful to integrate the system of equations analytically for a simple test case. Our simplified test case assumes that the dissociation time is constant in the interval  $0 \leq t \leq L_{QGP}$  and 0 if  $t > L_{QGP}$ , where  $L_{QGP}$  is the linear size of the fireball. The solution for the  $Q\bar{Q}$  mesons as a function of time is:

$$N_{Q\bar{Q}}^{\text{meson}}(0 \leq t \leq L_{QGP}; p_T, \nu) = N_{Q\bar{Q}}^{\text{hard}}(\text{quenched}; p_T, \nu) \frac{t_{\text{diss.}}(p_T)}{t_{\text{diss.}}(p_T) - t_{\text{form}}(p_T)} \left( e^{-t/t_{\text{diss.}}(p_T)} - e^{-t/t_{\text{form}}(p_T)} \right), \quad (32)$$

$$N_{Q\bar{Q}}^{\text{meson}}(t > L_{QGP}; p_T, \nu) = N_{Q\bar{Q}}^{\text{hard}}(\text{quenched}; p_T, \nu) \left[ \frac{t_{\text{diss.}}(p_T, \nu)}{t_{\text{diss.}}(p_T) - t_{\text{form}}(p_T)} \left( e^{-L_{QGP}/t_{\text{diss.}}(p_T)} - e^{-L_{QGP}/t_{\text{form}}(p_T)} \right) + \left( e^{-L_{QGP}/t_{\text{form}}(p_T)} - e^{-t/t_{\text{form}}(p_T)} \right) \right]. \quad (33)$$

The interested reader can easily deduce the solutions for  $N_{Q\bar{Q}}^{\text{hard}}(t; p_T, \nu)$  and  $N_{Q\bar{Q}}^{\text{diss.}}(t; p_T, \nu)$  and verify that the solutions in Eqs. 32, 33 are finite for  $t_{\text{form}}(p_T) = t_{\text{diss.}}(p_T)$ . Eqs. 32, 33 can be used to understand the qualitative features of the time dependence of quarkonium formation.

## B. Formation time of quarkonium states

The approach to estimating the formation time of quarkonium states differs considerably from the approach used for open heavy flavor[31, 32] or light particles [66] that come from the fragmentation of a hard parton. In the latter case the formation time is inversely proportional to the virtuality of the parton decay and is governed by longitudinal dynamics. For quarkonia, the  $Q\bar{Q}$  state is prepared instantly ( $\sim 1/\sqrt{p_T^2 + m_H^2}$ ) in the hard collision and subsequently expands to the spatial extent determined by the size of the asymptotic wavefunction. In this case all spatial directions are important. The velocity of the heavy quarks in the meson and a typical upper limit of the meson formation time can be evaluated as follows:

$$\beta_Q = \sqrt{\frac{\kappa^2}{\kappa^2 + m_Q^2}}, \quad t_{\text{rest frame}}^{\text{max}} = \frac{a_{\perp}}{\beta_Q}, \quad (34)$$

where the typical momenta,  $\kappa$  is related via Eq. 25 to  $k^2$  given the Tables I, II. The transverse sizes,  $a_\perp$ , are also given in Tables I, II. In this paper we are interested in high transverse momentum mesons, in which case there is a boost in the direction of propagation and, consequently, time dilation

$$t_{\text{form}}^{\text{max}}(p_T, \nu) = \gamma t_{\text{rest frame}}^{\text{max}}(\nu) = \gamma \frac{a_\perp}{\beta_Q}, \quad \gamma = \frac{\sqrt{p_T^2 + m_H^2}}{m_H}. \quad (35)$$

For example, for the relevant formation time determined by the expansion of the  $Q\bar{Q}$  state in a direction transverse to the direction of propagation the transverse size remains the same when boosted back to the laboratory frame but the velocity transforms by picking up a factor of  $1/\gamma$ . Note that in Eq. 35  $|\vec{p}| = p_T$  since in this paper we work at mid-rapidity. The masses of the quarkonium states  $m_H$  are taken from [67].  $\gamma$  is the meson boost factor. Since the formation process is non-perturbative and can not be modeled accurately, the values of  $t_{\text{form}}$  obtained from Eq. 35 should be considered as an estimate. We treat this as the upper limit of the formation time. In addition to calculating the final yields for  $t_{\text{form}} = t_{\text{form}}^{\text{max}} = \frac{\gamma a_\perp}{\beta_Q}$ , we also calculate the yields for  $t_{\text{form}} = t_{\text{form}}^{\text{min}} = \frac{\gamma a_\perp}{2\beta_Q}$  and the variation gives us an estimate of the uncertainty due to the uncertainty in the formation time.

### C. Dissociation time of quarkonium states

The propagation of a  $Q\bar{Q}$  state in matter is accompanied by collisional interactions mediated at the partonic level, as long as the momentum exchanges can resolve the partonic structure of the meson. Two effects are related to these interactions: a) a broadening of the distribution of quarkonium states relative to the original direction; b) a modification of the quarkonium wavefunction. The former effect integrates out as long as we consider inclusive production. The latter effect leads to the dissociation of the meson state.

Let us define:

$$\chi \mu_D^2 \xi = \int_{t_0}^t d\tau \frac{\mu_D^2(\mathbf{x}(\tau), \tau)}{\lambda_q(\mathbf{x}(\tau), \tau)} \xi, \quad \mathbf{x}(\tau) = \mathbf{x}_0 + \boldsymbol{\beta}(\tau - \tau_0). \quad (36)$$

In Eq. 36  $\mu_D^2$  is the typical squared transverse momentum transfer given by the Debye screening scale,  $\mu_D = gT$  for a gluon-dominated plasma.  $\chi$  is the opacity – the average number of collisions that the parton undergoes.  $\lambda_q$  is the mean scattering length of the quark and  $\xi \sim \text{few}$  is an enhancement factor from the power law tail of the differential scattering cross section. (Note that  $\xi$  is unrelated to  $\xi_q, \xi_g$  in Eq. 15 but appears also in transverse broadening due to cold nuclear effects in Eq. 18 since the basic formalism for momentum broadening is the same there.) Finally,  $\mathbf{x}_0$  is the position of the propagating  $Q\bar{Q}$  and  $\boldsymbol{\beta}$  is the velocity of the heavy meson. Note that  $|\boldsymbol{\beta}| < 1$ . For a medium of uniform parton density and length  $L$   $\chi \mu_D^2 \xi = \mu_D^2 (L/\lambda_q) \xi$ . For the realistic expanding medium the parton density and temperature can be determined as described in [68, 69] and the integral in Eq. 36 can be performed numerically.

With the results for the cumulative momentum transfer at hand, the medium-modified quarkonium wavefunction can be evaluated analytically for the functional form specified in Eq. 25. The survival probability for the closed heavy flavor mesons is given by

$$\begin{aligned} P_{\text{surv.}}(\chi \mu_D^2 \xi) &= \left| \frac{1}{2(2\pi)^3} \int d^2\mathbf{k} dx \psi_f^*(\Delta\mathbf{k}, x) \psi_i(\Delta\mathbf{k}, x) \right|^2 \\ &= \left| \frac{1}{2(2\pi)^3} \int dx \text{Norm}^2 \pi x(1-x) \Lambda^2 e^{-\frac{m_Q^2}{x(1-x)\Lambda^2}} \left[ \frac{2\sqrt{x(1-x)\Lambda^2} \sqrt{\chi \mu_D^2 \xi + x(1-x)\Lambda^2}}{\sqrt{x(1-x)\Lambda^2 + \sqrt{\chi \mu_D^2 \xi + x(1-x)\Lambda^2}}} \right] \right|^2. \end{aligned} \quad (37)$$

The dissociation rate for a given meson is then given by

$$t_{\text{diss.}}(p_T) = \frac{dP_{\text{diss.}}(p_T)}{dt} = -\frac{dP_{\text{surv.}}(p_T)}{dt} \quad (38)$$

The uncertainty in  $t_{\text{diss}}$  arises from the uncertainty in the coupling between the heavy quarks and the medium (described by the strong coupling constant  $g$ ) and the enhancement that arises from the power law tails of the Moliere multiple scattering in the Gaussian approximation to transverse momentum diffusion [31] (described by  $\xi$ ). In our calculations we use two sets  $g = 1.85$ ,  $\xi = 2$  and  $g = 2$ ,  $\xi = 3$  to understand the sensitivity of the results to these parameters.

To get a sense of the formation and dissociation times involved in the quarkonium dynamics in the QGP, we give the values for a fixed transverse momentum  $p_T = 10$  GeV for the quarkonium states and consider their production in

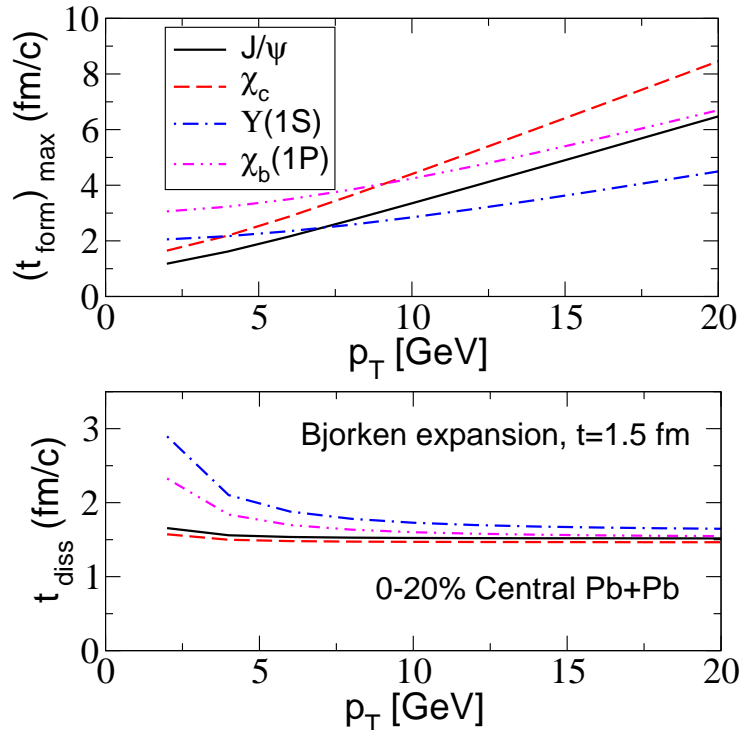


FIG. 3: (Color online) Top panel: formation time for selected charmonium ( $J/\psi$ ,  $\chi_c$ ) and bottomonium ( $\Upsilon(1S)$ ,  $\chi_b(1P)$ ) versus transverse momentum. Bottom panel: the corresponding dissociation times quoted at  $t = 1.5$  fm/c for a hard process in the center of the collision geometry, 0-20% Pb+Pb reactions at the LHC.

the center of the collision geometry. The specific nuclear collisions that we chose are 0-20% central Au+Au collisions at RHIC at  $\sqrt{S_{NN}} = 0.2$  TeV. In the examples in Table III and Table IV  $g = 2$  and  $\xi = 2$ . The results include the boost factor. Since the medium expands after the collision, we quote the formation and dissociation times at  $t = 1.5$  fm/c. Results for charmonia and bottomonia are presented in Table III and Table IV, respectively.

To clarify the  $p_T$  dependence of the formation and dissociation times we show in Fig. 3,  $t_{\text{form}}$  and  $t_{\text{diss}}$  at  $t = 1.5$  fm/c for 0 – 20% Pb+Pb collisions for 2.76 TeV collisions at the LHC.

Charmonium state	$J/\psi$	$\chi_{c0,1,2}$
$(t_{\text{form}})_{\text{max}}$ [fm/c]	3.35	4.40
$t_{\text{diss}}$ [fm/c]	1.74	1.61

TABLE III: Upper limit on the formation time and dissociation time of quarkonium states of  $p_T = 10$  GeV and produced in the center of the nuclear overlap region of 0-20% central Au+Au collisions at RHIC.

Bottomonium state	$\Upsilon(1S)$	$\Upsilon(2S)$	$\Upsilon(3S)$	$\chi_{b0,1,2}(1)$	$\chi_{b0,1,2}(2)$	$\chi_{b0,1,2}(3)$
$(t_{\text{form}})_{\text{max}}$ [fm/c]	1.44	2.85	4.17	2.36	3.45	6.23
$t_{\text{diss}}$ [fm/c]	3.30	2.23	1.93	1.93	2.06	1.73

TABLE IV: Upper limit on the formation time and dissociation time of bottomonium states of  $p_T = 10$  GeV and produced in the center of the nuclear overlap region of 0-20% central Au+Au collisions at RHIC.

#### D. Quenching of the color-octet state

Before the formation of the overall color neutral wavefunction on a time scale of  $t_{\text{form}}$ , the  $Q\bar{Q}$  state has both color-singlet and color-octet components. In fact, from Section II we know that the dominant contribution to quarkonium production comes from the color octet state.

Therefore, from the hard proto-quarkonium creation to the formation of the quarkonium wavefunction, the color octet state undergoes energy loss, and consequently quenching, as it passes through the medium. This can be thought of as a very massive gluon moving through the QGP for  $t_{\text{form}}$ .

The quenching for massive partons traversing the QGP has been extensively investigated. Starting with the discussion of the dead-cone effect [70], the effect of mass has been incorporated in all energy loss approaches. We include the quenching effect in the calculation of  $R_{AA}$  by calculating the quenching factor for a ‘‘gluon’’ of mass  $2m_Q$  traversing the medium for a time  $t_{\text{form}}$ . The details of the GLV formalism used for the energy loss calculation can be found in [71]. In our calculation, we incorporate the fluctuations of the energy loss due to the multiple gluon emission and the diffuseness of the nuclear geometry (fluctuations in path length).

Starting with the yields obtained in Section II, (including CNM effects described in Section III), this energy loss leads to a quenching of the yield. This quenched yield for the color-octet states give the initial conditions for the rate equations that take into account the dissociation dynamics. The color-singlet components are, of course, unquenched.

## VI. NUMERICAL RESULTS FOR THE NUCLEAR MODIFICATION FACTORS

### A. $R_{AA}$ for $J/\psi$ and $\Upsilon(1S)$

In this section we neglect the Cronin effect but include initial-state cold nuclear matter energy loss and shadowing. Let us first consider the nuclear modification factor for  $J/\psi$  mesons. From Fig. 4 we see that the data on  $R_{AA}$  in RHIC Au+Au collisions [72] shows a  $R_{AA}$  roughly between 0.5 and 0.75 at  $p_T \sim 6$  GeV. On the other hand, Cu+Cu collisions [56] show a  $R_{AA}$  greater than 1. Both measurements have large error bars. Within the uncertainty in our model parameters, we obtain results consistent with RHIC data, albeit systematically slightly smaller than the measured  $R_{AA}$  (for  $p_T \sim 6$  GeV,  $R_{AA} \sim 0.35 - 0.45$  for Au+Au and  $R_{AA} \sim 0.45 - 0.65$  for Cu+Cu). In Fig. 4, our results for the prompt yields of  $J/\psi$  mesons are marked by upper and lower yellow bands corresponding to the upper ( $t_{\text{form}}^{\text{max}}$ ) and lower ( $t_{\text{form}}^{\text{min}} = t_{\text{form}}^{\text{max}}/2$ ) limits of our formation time estimate respectively. The bands themselves correspond to our estimate of the uncertainty in the sets of parameters that determine the coupling of the heavy quarks with the in-medium partons [ $g = 1.85$ ,  $\xi = 2$  (minimum considered coupling gives the upper limit of the yellow band) and  $g = 2$ ,  $\xi = 3$  (maximum considered coupling for the lower limit of the yellow band)]. The pronounced effect of the variation of the formation time can be intuitively seen as follows. From Eq. 28, we see that the dissociation mechanism is operative only when  $N_{QQ}^{\text{meson}}$  is substantial, i.e. after  $t_{\text{form}}$ . Since the upper limit for formation time of quarkonia can be on the order of several fm/ $c$ , (see Tables III, IV), the density of the medium at  $t_{\text{form}}^{\text{max}}$  is reduced considerably due to Bjorken expansion, giving weaker dissociation and weaker suppression. This effect is more pronounced than the details of the coupling of heavy quarks to the in-medium partons.

The RHIC experiments report suppression for the inclusive  $J/\psi$  yield. For direct comparisons, we also show the  $R_{AA}$  for the inclusive yields in Fig. 4 with dashed lines. The color scheme for the various parameters is analogous to the direct production, though we do not color in yellow the band associated with the uncertainty in coupling to avoid cluttering. The  $B$ -meson yields for p+p and A+A collisions were taken from [32].

The high- $p_T$  suppression of  $J/\psi$  mesons in Pb+Pb collisions at the LHC, reported by the ATLAS and CMS experiments, is substantially higher than the RHIC results. For example, for  $p_T \in (6.5, 30)$  GeV, CMS [73] shows  $R_{AA} \sim 0.2$  for the most central collisions. For a sharply falling spectrum we expect the suppression to be dominated by the low momenta in the  $p_T$  bin. (The mean  $p_T$  of the observed particles in the bin is roughly 9.3 GeV, for p+p collisions.) On general grounds, one expects the suppression at LHC to be larger than at RHIC. The initial temperature at LHC is higher than at RHIC, and consequently the gluon density at any given time in the Bjorken expansion is also higher. This will give rise to more rapid dissociation at LHC both in equilibrium and non-equilibrium approaches. (The system sizes for Au+Au and Pb+Pb collisions are roughly the same.)

For  $p_T = 9$  GeV at the LHC, our calculations give  $R_{AA} \sim 0.3 - 0.4$ , which is slightly smaller than at RHIC (at the same  $p_T$ ) but underestimates the observed suppression at LHC in the most central Pb+Pb collisions. The ATLAS experiment has presented the ratio of binary collision scaled central-to-peripheral  $J/\psi$  yields  $R_{CP}$  [74]. More specifically, their baseline is given by the 40-80% peripheral Pb+Pb reactions. The  $p_T$  cuts used to obtain ATLAS results are such that 80% of the yields come from  $p_T > 6.5$  GeV. Comparison to the theoretical model calculation is shown in the left bottom panel of Fig. 4. The two data points are for 0-10% and 10-20% centrality. The CMS prompt  $J/\psi$   $R_{AA}$  result [73] is shown in right bottom panel of Fig. 4. The two data points are again for 0-10% and 10-20% centrality and exhibit stronger suppression than our theoretical model predictions. The ALICE experiment at LHC has measured the nuclear modification of  $J/\psi$  production at forward rapidity [75] and low transverse momentum. To constrain theoretical models of quarkonium production in heavy ion collisions, it will be very helpful to extend these forward rapidity data to high transverse momentum.

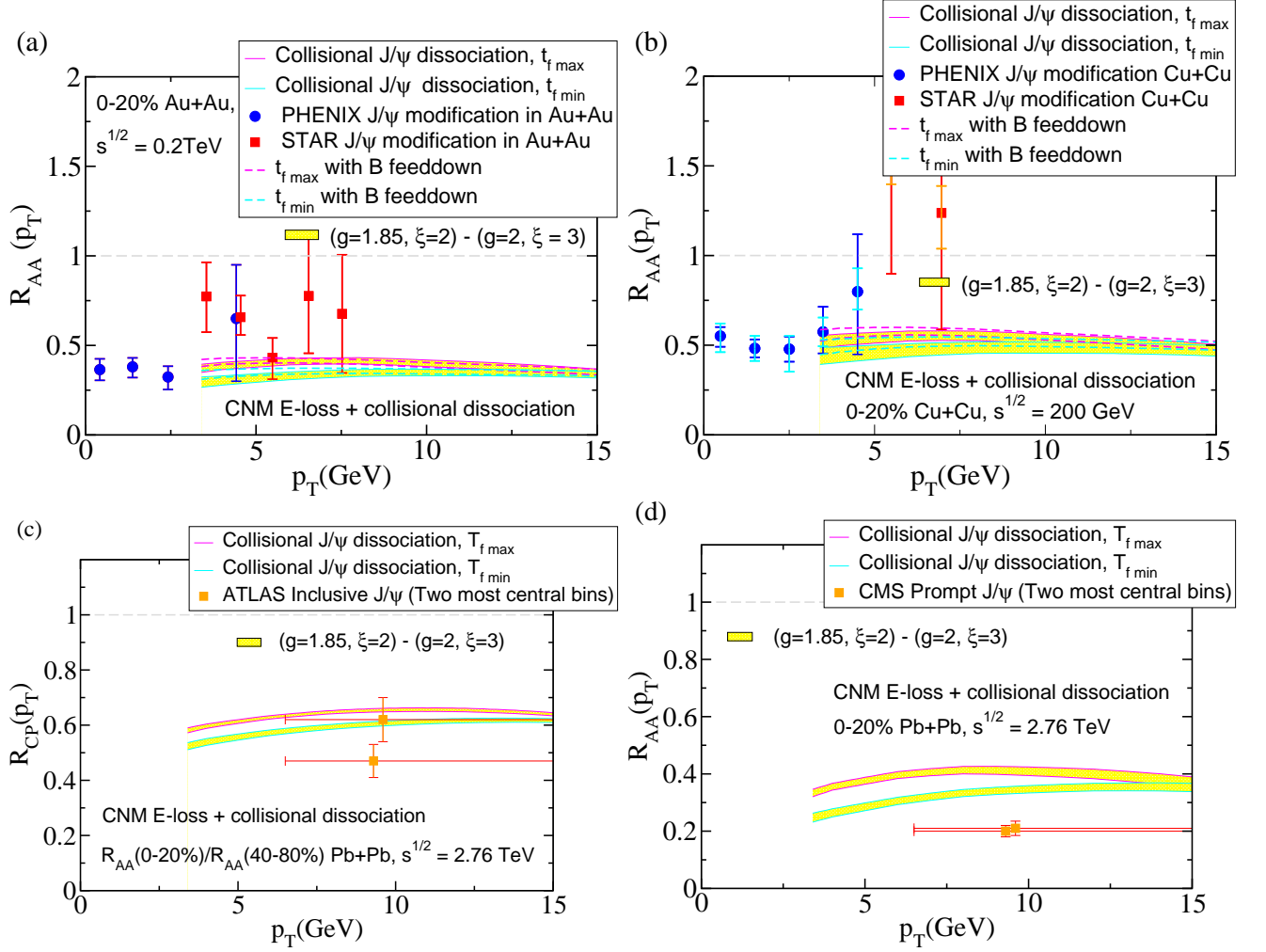


FIG. 4: (Color online) Theoretical model predictions for  $J/\psi$   $R_{AA}$  in 0-20% central nucleus-nucleus collisions. The top left panel is for RHIC Au+Au collisions at  $\sqrt{S} = 0.2$  TeV [72]. The top right panel is for RHIC Cu+Cu collisions at  $\sqrt{S} = 0.2$  TeV [56]. The lower panels are for LHC Pb+Pb collisions at  $\sqrt{S} = 2.76$  TeV [73, 74]. The various curves represent the uncertainty due to variations in  $g$  and  $\xi$  (taking the sets  $g = 1.85$ ,  $\xi = 2$  and  $g = 2$ ,  $\xi = 3$ ), and a factor of 2 variation in  $t_{\text{form}}$ . In the lower left panel [panel (c)] the lower data point corresponds to 0 – 10% most central events and the other to 10 – 20%. These results neglect the Cronin effect. Dashed curves include the  $B \rightarrow J/\psi$  feed-down.

In our formalism, we have approximated the quarkonium wavefunction by the vacuum wavefunction, which is valid if the thermal effects on the quarkonium wavefunctions are small. The thermal wavefunctions (for example, those obtained by solving the Schrödinger equation with thermal potentials [2, 8–10]) will be wider in position space at higher temperature and therefore will dissociate more easily. Therefore a stronger suppression at LHC could be the evidence for thermalization effects at the level of the quarkonium wavefunction. We leave a more detailed analysis of thermal effects on the wavefunctions for future work. Nevertheless, it is important to identify at what centrality the discrepancy between the present theoretical model predictions and the data appear. In Fig. 5 we show the  $p_T$ -averaged suppression,

$$R_{AA}(N_{\text{part}}) \text{ (or } R_{CP}(N_{\text{part}})) = \frac{\int_{p_{\text{min.}}} dp_T R_{AA}(p_T; N_{\text{part}}) \text{ (or } R_{CP}(p_T; N_{\text{part}})) \frac{d\sigma}{dy dp_T}}{\int_{p_{\text{min.}}} dp_T \frac{d\sigma}{dy dp_T}}, \quad (39)$$

of  $J/\psi$  mesons versus centrality. We present a comparison to the ATLAS central-to-peripheral data [74] in the left panel. The deviation between data and theory is only seen for  $N_{\text{part}} > 300$ . A comparison to the CMS data [73] is shown in the right panel. In this case the deviation between data and theory is seen for  $N_{\text{part}} > 200$ .

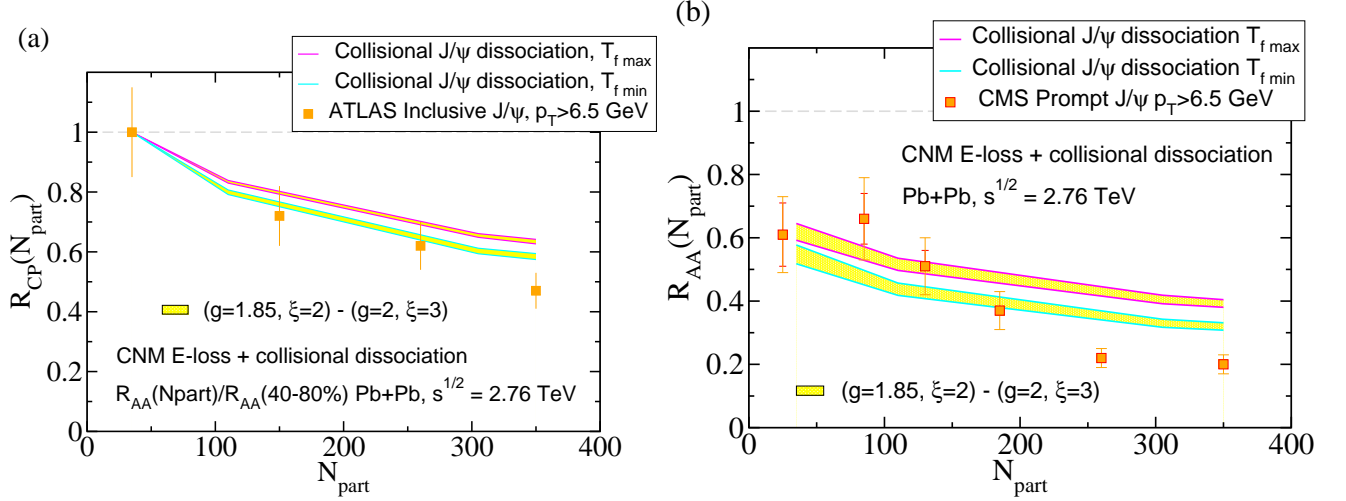


FIG. 5: (Color online) Expected  $J/\psi$  suppression versus centrality ( $N_{\text{part}}$ ) at  $\sqrt{S} = 2.76$  TeV. The left panel compares the theoretical results to the ATLAS  $R_{\text{CP}}$  data [74]. The right panel compares the theoretical results to the CMS  $R_{\text{AA}}$  data [73].

The CMS experiment at the LHC has also measured  $R_{\text{AA}}$  for  $\Upsilon(nS)$  states in Pb+Pb collisions at  $\sqrt{S} = 2.76$  TeV per nucleon pair. The result [76] is presented for decay muons satisfying the transverse momentum cut  $p_T(\mu^\pm) > 4$  GeV and rapidity  $|\eta| < 2.4$ .

$$\begin{aligned} \frac{\Upsilon(2S+3S)}{\Upsilon(1S)}|_{pp} &= 0.76^{+0.16}_{-0.14} \pm 0.12, \\ \frac{\Upsilon(2S+3S)}{\Upsilon(1S)}|_{PbPb} &= 0.24^{+0.13}_{-0.12} \pm 0.02, \end{aligned} \quad (40)$$

giving

$$\frac{R_{\text{AA}}(\Upsilon(2S+3S))}{R_{\text{AA}}(\Upsilon(1S))} = 0.32^{+0.19}_{-0.15} \pm 0.03. \quad (41)$$

We cannot calculate the equivalent ratio of  $R_{\text{AA}}$ s because our formalism for the production and propagation of  $\Upsilon$ s is not applicable to  $p_T(\Upsilon) \lesssim 6$  GeV. In our approach the meson should be boosted relative to the medium. Furthermore, for static or slowly moving mesons one may expect thermal effects on the quarkonium wavefunction. These are precisely the  $\Upsilon$ s that determine the total yield ratios in Eqs. 40, (41).

For  $p_T > 7$  GeV at the LHC, our calculations show that  $\frac{R_{\text{AA}}(\Upsilon(2S+3S))}{R_{\text{AA}}(\Upsilon(1S))} \sim 1$  (the lower panels of Fig. 6). Physically, this is because the higher dissociation rate for the excited mesons is compensated by their larger formation time, which means that dissociation becomes dominant after the medium has diluted. If in future experiments  $p_T$ -differential yields of  $\Upsilon(2S+3S)$  shows a much stronger suppression compared to  $\Upsilon(1S)$  for  $p_T \gtrsim 7$  GeV, that may also support the possibility for thermal effects on the quarkonium wavefunction at high  $p_T$ . This is because the thermal wavefunctions of higher excited states, being broader in position space, are more easily affected by the QGP, thereby naturally giving even higher dissociation rates. Fig. 6 also shows theoretical predictions for the suppression of the various  $\Upsilon$  states in central Au+Au and Pb+Pb collisions at RHIC and the LHC, respectively. In the top right panel we present a comparison to the minimum bias  $p_T$ -differential  $\Upsilon(1S)$  CMS nuclear modification data. In this case, the theoretical calculation is performed for the average number of participants for minimum bias collisions.

The overall suppression of the  $J/\psi$  and the  $\Upsilon$  yields in A+A collisions is a combination of CNM and QGP effects. In this section we ignored transverse momentum broadening effects. Therefore, the suppression is largely due to cold nuclear matter energy loss and QGP dissociation (the effect of shadowing is small). In Section VI B, we will show results for A+A collisions including Cronin, and results for p+A collisions where QGP effects are absent. (See Fig. 8 for  $J/\psi$  and Fig. 9 for  $\Upsilon$ .) For  $p_T \sim 6$  GeV,  $R_{pA} \sim 0.8$  for both  $J/\psi$  and  $\Upsilon$ . Noting that in A+A collisions the CNM effects are amplified relative to p+A, we conclude that a significant part of the suppression in quarkonium yield in our calculation comes from cold nuclear matter energy loss. The situation is more complicated when we include transverse momentum broadening as we discuss next.

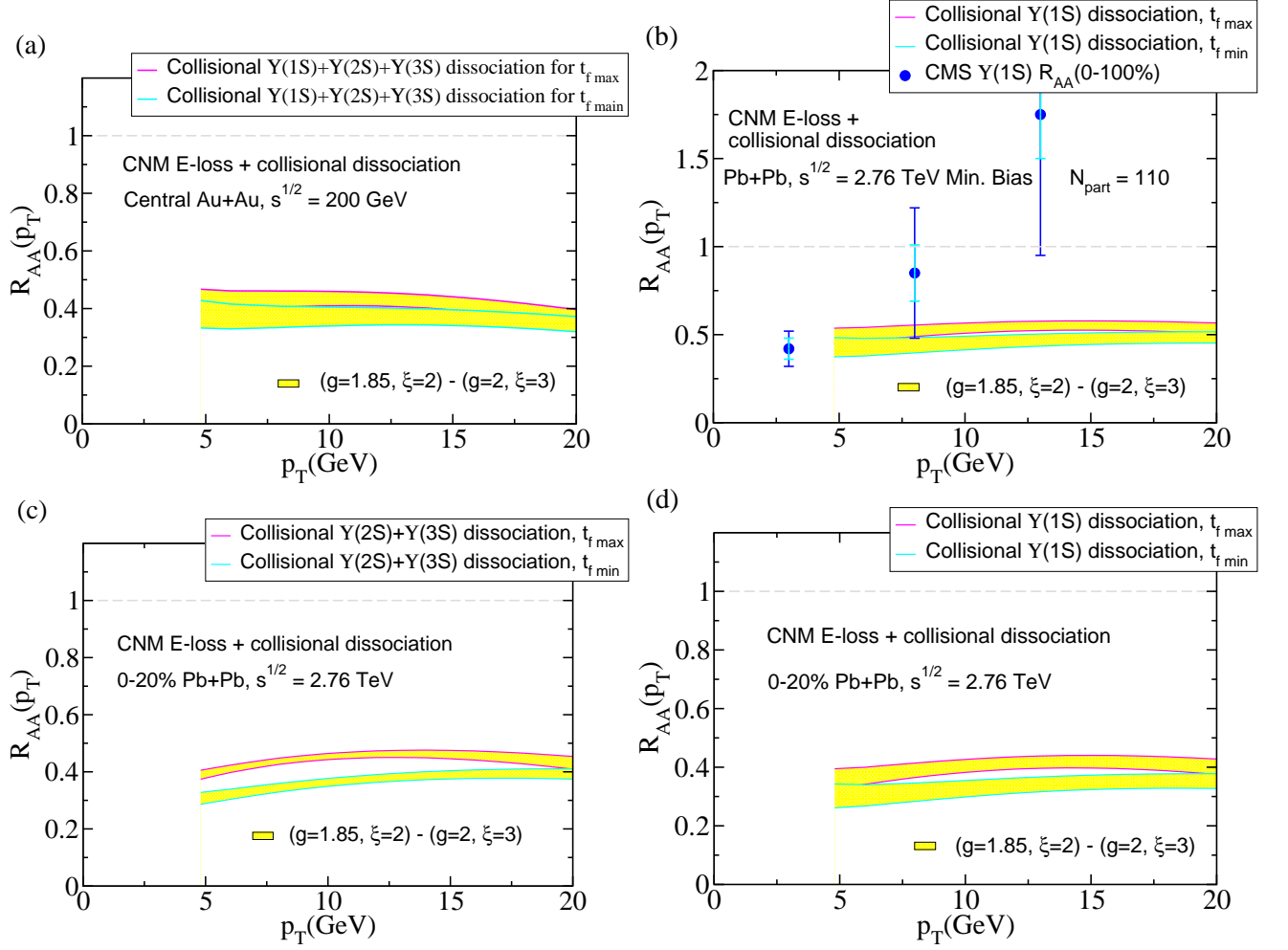


FIG. 6: (Color online) Theoretical model predictions for  $\Upsilon R_{AA}$  in nucleus-nucleus collisions. The top right panel is for minimum bias collisions and the rest for 0-20% central collisions. The top left panel shows  $R_{AA}$  results for  $\Upsilon(1S) + \Upsilon(2S) + \Upsilon(3S)$  in Au+Au at  $\sqrt{S} = 0.2$  TeV. The bottom left and right panels shows  $R_{AA}$  results for  $\Upsilon(2S) + \Upsilon(3S)$  and  $\Upsilon(1S)$ , respectively, in Pb+Pb at  $\sqrt{S} = 2.76$  TeV. The top right panel data from CMS is for 0 – 100% centrality [73] compared to the theoretical prediction at the minimum bias  $N_{\text{part}} \approx 110$ .

### B. Transverse momentum broadening effects

As expected, transverse momentum broadening effects enhance the production of  $J/\psi$  mesons for  $p_T \sim 5 - 10$  GeV in heavy ion collisions (Fig. 7). The Cronin effect is not very important for  $p_T \gtrsim 10$  GeV at these center-of-mass energies. The main features are as follows: the Cronin effect can substantially alter the  $R_{AA}$  of  $J/\psi$  mesons with  $p_T \sim 7$  GeV at RHIC. For example, for Au+Au collisions  $R_{AA}$  increases from  $\sim 0.35 - 0.45$  to  $\sim 0.8 - 1.2$ . For Cu+Cu collisions  $R_{AA}$  increases from  $\sim 0.45 - 0.65$  to  $\sim 0.7 - 1.0$ . The reason behind this enhancement is that the mean scattering lengths of the initial-state gluons (which dominate quarkonium production) are considerably smaller than the mean scattering lengths for quarks. The Cronin effect at the LHC is smaller than the Cronin effect at RHIC because of the harder quarkonium spectrum. Including broadening only increases  $R_{AA}$  at  $p_T \sim 7$  GeV from  $\sim 0.3 - 0.4$  to  $\sim 0.6 - 0.8$ . The theoretically calculated  $R_{AA}$  for  $J/\psi$  may be consistent with the RHIC Cu+Cu results but is only marginally compatible with the RHIC Au+Au results for  $p_T$  above 4 GeV. Also, it is clearly incompatible with the ATLAS central-to-peripheral Pb+Pb data at the LHC and the CMS  $R_{AA}$  suppression. The differences in the degree of  $p_T = 5 - 10$  GeV suppression of quarkonium production between RHIC and the LHC in Fig. 7 suggest that better understanding of the Cronin effect (if any) is necessary for consistent  $J/\psi$  phenomenology in heavy ion collisions.

More specifically, experimental quarkonium yields in p+A or d+A collisions, where effects from the QGP are absent,

are important to constrain the cold nuclear matter effects. Our theoretical predictions for the high- $p_T$   $J/\psi$  nuclear modification factor  $R_{pA}$  in such collisions are given in Fig. 8. The upper (solid red) curve includes the Cronin effect. The lower (solid blue) curve includes only power corrections and CNM energy loss. The upper curve is the maximum Cronin enhancement we obtain for reasonable parameters and therefore the band should be interpreted as the plausible region for  $R_{pA}$ . Comparison with recent PHENIX data [79] suggests that the  $R_{pA}$  is closer to the lower curves (no Cronin). LHC  $R_{AA}$  measurements also point to an absence of the Cronin effect for quarkonia. One interesting point to note is that the Cronin peak in  $AA$  is smaller than  $pA$  collisions due to the QGP effects. We finally point out that including the contribution from  $B$  decays reduces the Cronin enhancement for  $p_T \sim 5 - 10$  GeV slightly.

The combined results for  $R_{AA}$  (0-20% central) and  $R_{pA}$  (minimum bias) for bottomonia are given in Fig. 9. The effect of transverse momentum broadening is much smaller for bottomonia when compared to the one for charmonia. This can be intuitively understood as follows. The mechanism for Cronin enhancement in this calculation is that initial state scattering increases the typical transverse momentum carried by the incident partons by a few GeV. For quarkonia, there is an additional scale  $m_H$ . For bottomonia the mass scale is considerably larger than the transverse momentum broadening scale and few additional GeV do not increase the yields significantly. Preliminary  $\Upsilon$  suppression data are now available at RHIC [77]. More differential  $p_T$  data will shed light on the similarities and differences in the CNM effects at RHIC and at the LHC.

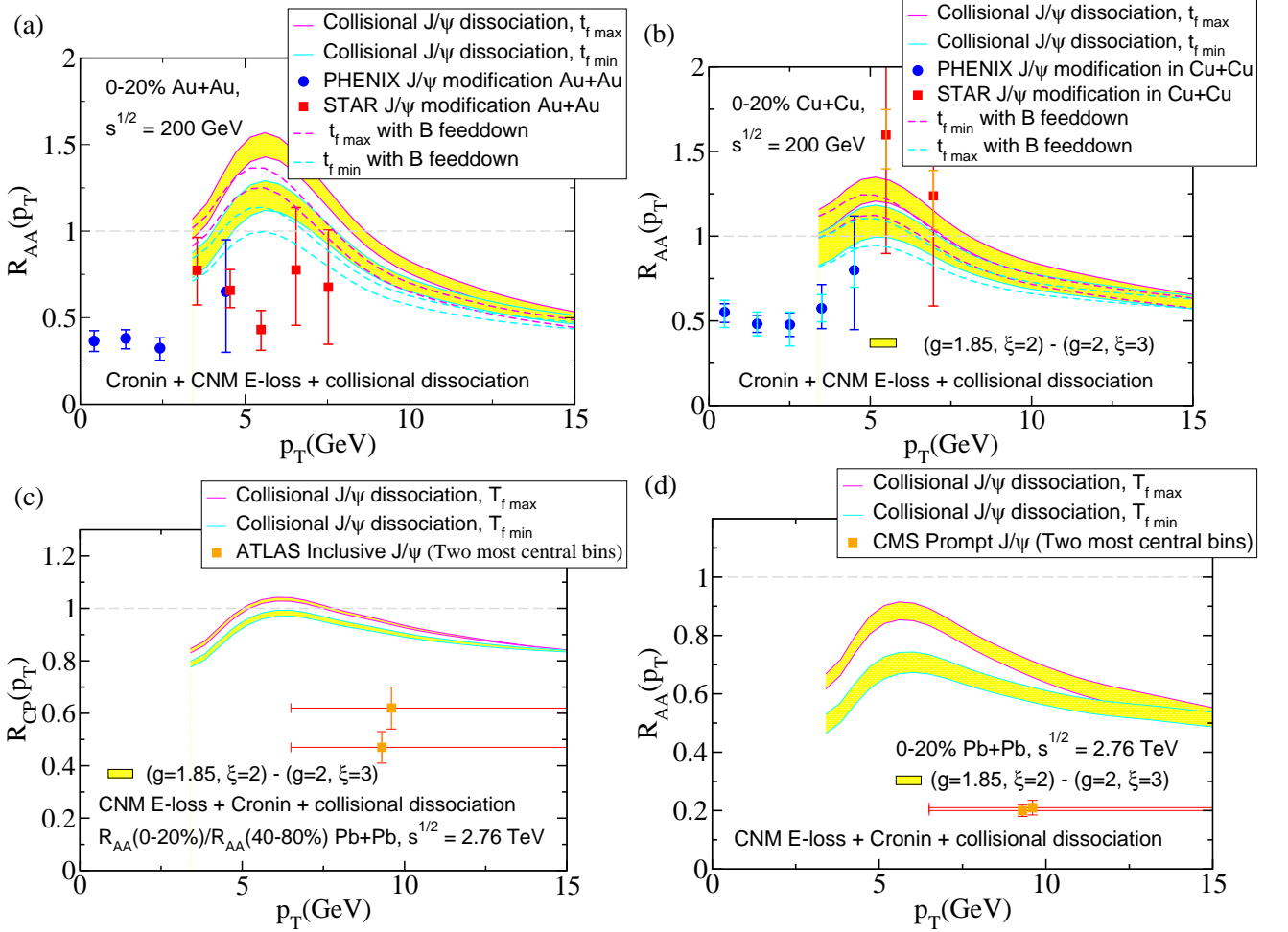


FIG. 7: (Color online) Theoretically calculated  $R_{AA}$  for  $J/\psi$ , including the Cronin effect. The top left panel is for RHIC Au+Au collisions at  $\sqrt{s} = 0.2$  TeV. The top right panel is for RHIC Cu+Cu collisions at  $\sqrt{s} = 0.2$  TeV. The lower two panels are for LHC Pb+Pb collisions at  $\sqrt{s} = 2.76$  TeV as in Fig. 4.

## VII. CONCLUSIONS

In summary, we carried out a detailed study of high transverse momentum quarkonium production and modification in heavy ion reactions at RHIC and at the LHC. We used a NRQCD approach to calculate the baseline quarkonium cross sections. We found that for  $J/\psi$  mesons the theoretically computed spectrum is slightly harder than the one observed in the experiment. For all  $\Upsilon$  states ( $1S, 2S, 3S$ ) the agreement is within a factor of two when we consider both the TeVatron and the LHC data. In reactions with heavy nuclei, we presented theoretical model calculations for the nuclear modification of quarkonium yields at high  $p_T$  in minimum bias p(d)+A and 0-20% central A+A collisions. We focused on the consistent inclusion of both cold (CNM) and hot (QGP) nuclear matter effects in different colliding systems at different center-of-mass energies. We compared our results to published and preliminary experimental data, where applicable.

In calculating the spectra of quarkonia in heavy ion reactions, we included nuclear shadowing (here implemented as coherent power corrections) and initial-state energy loss. We also provided, to the best of our knowledge, the first implementation of initial-state transverse momentum broadening to study phenomenologically a possible Cronin-like enhancement for quarkonia. All these effects have been well studied for light partons and have been recently incorporated in open heavy flavor production. In this paper we extended them to  $J/\psi$  and  $\Upsilon$  mesons. Since the  $Q\bar{Q}$  pair is created in the short-distance hard scattering process and evolves quickly into a component of the quarkonium wavefunction, the effects of propagation through the QGP were included through (a) quenching of the color octet

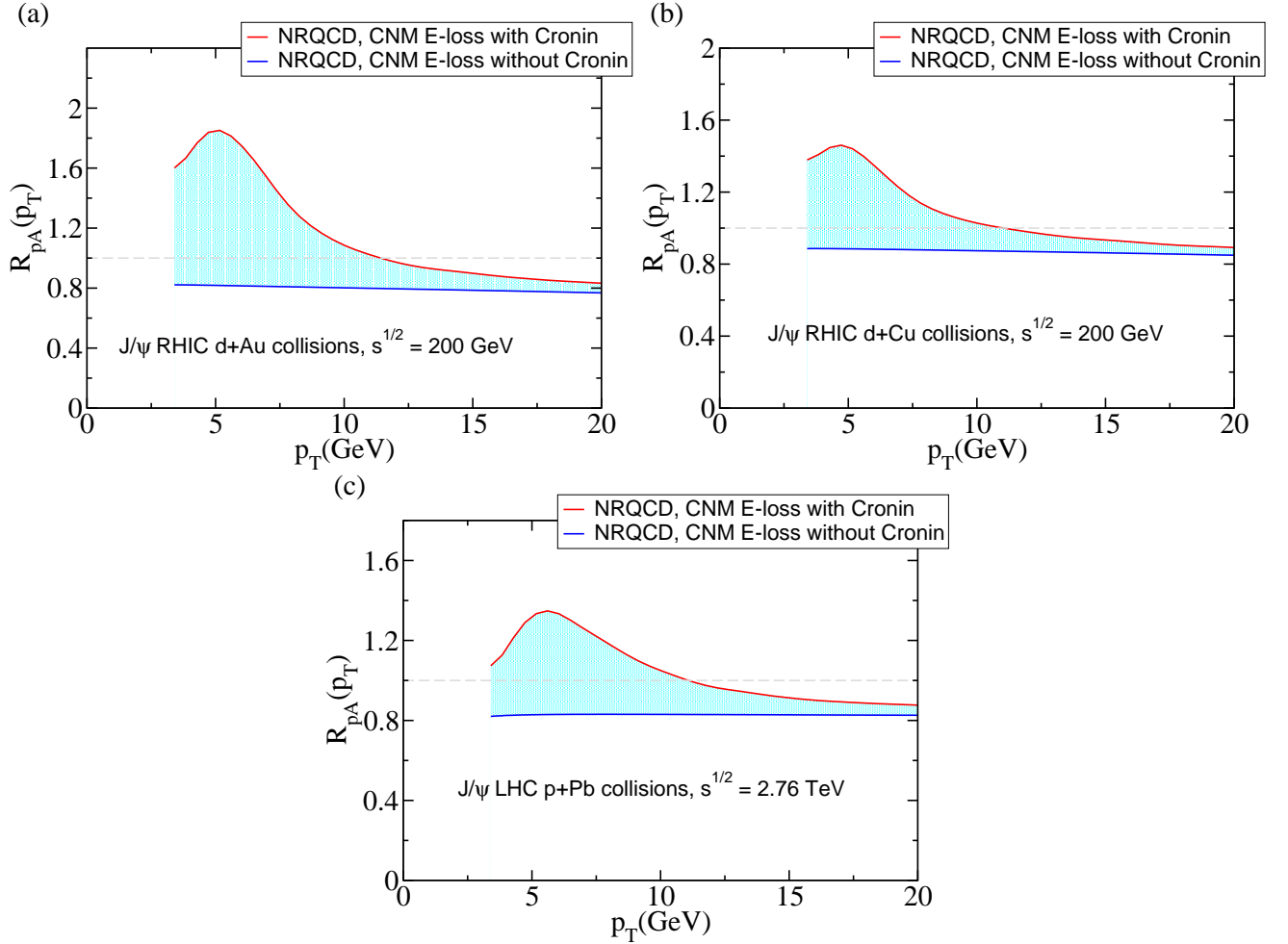


FIG. 8: (Color online) Theoretical predictions for  $J/\psi$   $R_{pA}$  in minimum bias collisions with (upper curve, red online) and without (lower curve, blue online) the Cronin effect. In this plot we only show the prompt yields. The top left panel is for RHIC d+Au collisions at  $\sqrt{s} = 0.2$  TeV. The top right panel is for RHIC d+Cu collisions at  $\sqrt{s} = 0.2$  TeV. The lower panel is for LHC p+Pb collisions at  $\sqrt{s} = 2.76$  TeV.

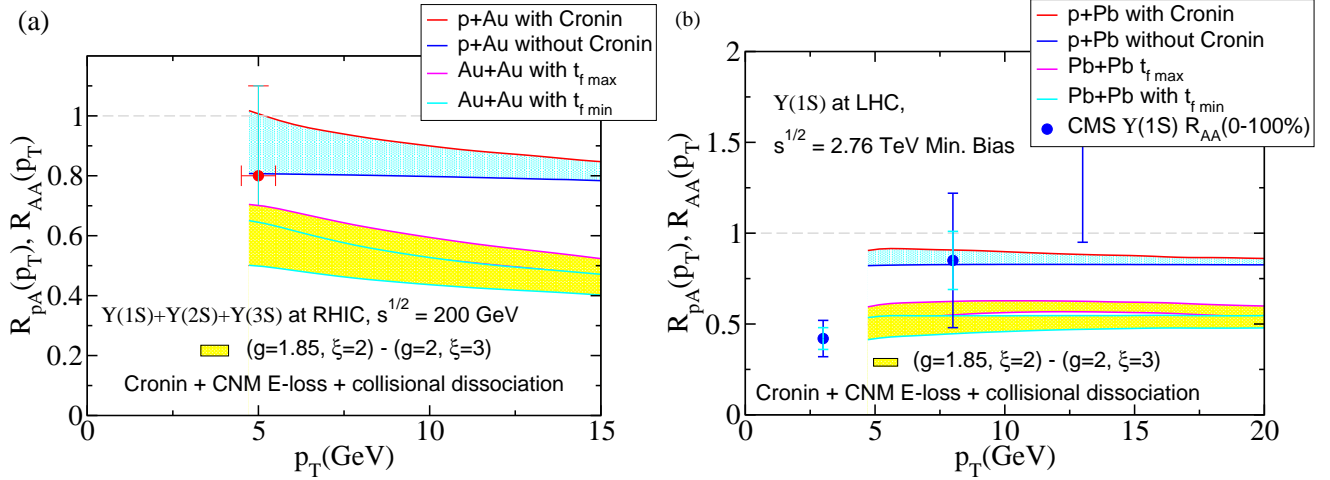


FIG. 9: (Color online) Theoretical model predictions for minimum bias  $R_{pA}(\Upsilon)$  and for  $R_{AA}(\Upsilon)$ . The left panel is for RHIC p+Au and central (0 – 20%) Au+Au collisions at  $\sqrt{S} = 0.2$  TeV. Data is from STAR [77]. The right panel is for LHC p+Pb and minimum bias ( $N_{\text{part}} \approx 110$ ) Pb+Pb collisions at  $\sqrt{S} = 2.76$  TeV. Data is from CMS [73].

component (b) collisional dissociation model for the formed meson, which was successful in describing the attenuation of open heavy flavor,  $B \rightarrow \ell + X, D \rightarrow \ell + X$ , at RHIC. In this paper we restricted our results to high transverse momentum and explored the consequences of assuming that the initial wavefunctions of the quarkonia are well approximated by vacuum wavefunctions in the short period before the dissociation.

We found that ignoring the Cronin effect leads to a small overestimate of the suppression of  $J/\psi$  mesons in the  $p_T$  region between 5 GeV and 10 GeV in central Cu+Cu and Au+Au collisions at  $\sqrt{S} = 0.2$  TeV at RHIC. Including initial-state transverse momentum broadening leads to a somewhat better agreement between theory and the current experimental data only for the Cu+Cu reactions. A smaller Cronin enhancement will work better. We demonstrated that CNM effects can be easily constrained in d+A reactions at RHIC. For example, the d+Au calculation that includes power corrections and cold nuclear matter energy loss predicts 20% suppression of the  $J/\psi$  cross section. Including transverse momentum broadening may lead to as much as 50% enhancement in the region of the Cronin peak. We also found that the Cronin-like modification of the  $\Upsilon$  spectrum is much smaller. Current data on high- $p_T$  quarkonium production at RHIC does not indicate the presence of thermal effects at the level of the quarkonium wavefunction within our theoretical framework.

The conclusions from our theoretical model comparison to the  $\sqrt{S} = 2.76$  TeV LHC data are not as clear cut. Our calculations underestimated the suppression for  $J/\psi$  production reported by the ATLAS and CMS experiments in the most central Pb+Pb collisions. On the other hand, they agree quite well in mid-central and peripheral reactions. We found that the Cronin enhancement at the LHC is smaller than the one at RHIC due to the harder spectra. However, any Cronin enhancement appears incompatible with the experimental results. For  $\Upsilon$  mesons,  $p_T$ -differential data in A+A collisions is scarce. CMS data for minimum bias  $\Upsilon(1S)$  indicate that the low  $p_T$  suppression may decrease or disappear at high  $p_T$ . At the same time, at low  $p_T$ , where our calculation is not applicable, CMS reported a strong relative suppression of  $\Upsilon(2S + 3S)$  to  $\Upsilon(1S)$ . If the data is extended to high  $p_T$  with similar results, it will clearly be incompatible with our model predictions with quarkonium wavefunctions unaffected by thermal effects. Together with a more refined  $p_T$ -differential data on  $J/\psi$  suppression at  $\sqrt{S} = 2.76$  TeV, this will be a strong indication that thermal QGP effects may persist for high transverse momentum quarkonia at the LHC in central Pb+Pb reactions. We plan to address this possibility in a separate publication.

## VIII. ACKNOWLEDGMENTS

The authors acknowledge e-mail communication with E. Braaten. The authors also thank T. Dahms, A. Dainese, C. Mironov and an anonymous referee for useful comments. This research is supported by National Sciences and Engineering Research Council of Canada (NSERC), the US Department of Energy, Office of Science, under Contract No. DE-AC52-06NA25396 and in part by the JET collaboration.

Appendix A: Fitting color-octet matrix elements for charmonia and a baseline for LHC at  $\sqrt{S} = 2.76$  TeV

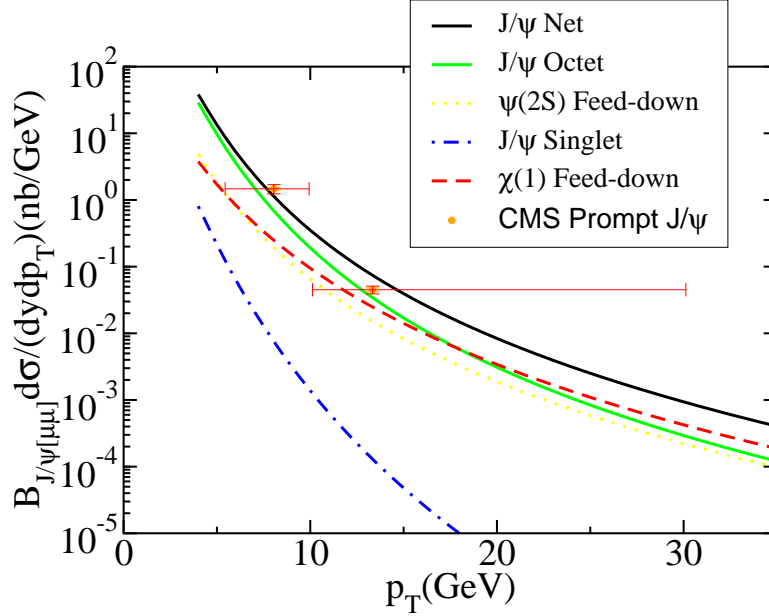


FIG. 10: (Color online) The cocktail of contributions that gives the p+p yield for  $J/\psi$  production at the LHC at  $\sqrt{S} = 2.76$  TeV. The uppermost curve (black online) gives the net yield and gives the p+p baseline. We see that the dominant contribution is the color-octet contribution. The data is from CMS [73].

For the net production of  $J/\psi$  we consider the direct contribution, and feed-down contributions from  $\chi_{c0}(1P)$ ,  $\chi_{c1}(1P)$ ,  $\chi_{c2}(1P)$  and  $\psi(2S)$ . The relevant branching fractions are given in Table V [67],

meson from	to $\chi_{c0}$	to $\chi_{c1}$	to $\chi_{c2}$	to $J/\psi$
$\psi(2S)$	0.0962	0.092	0.0874	0.595
$\chi_{c0}$				0.0116
$\chi_{c1}$				0.344
$\chi_{c2}$				0.195

TABLE V: Relevant branching fractions for charmonia [67].

$p_T$ -differential yields at small rapidity for  $J/\psi$  is available from LHC([54, 73]), TeVatron ([50, 53]) and RHIC ([55, 56]). Yields of  $\psi(2S)$  have been measured at TeVatron ([52, 53, 61]) and LHC([62]). Data for  $\chi_{cJ}$  is available from TeVatron [53].

The following color-singlet and color-octet contributions are relevant for our calculation.

1. Direct contributions

$$\begin{aligned}
 \mathcal{M}(\psi[{}^3S_1]_1) &= \langle \mathcal{O}(c\bar{c}([{}^3S_1]_1) \rightarrow J/\psi) \rangle = 3N_c \frac{|R_{n=1}(0)|^2}{2\pi} \\
 \mathcal{M}(\psi[{}^3S_1]_8) &= \langle \mathcal{O}(c\bar{c}([{}^3S_1]_8) \rightarrow J/\psi) \rangle \\
 \mathcal{M}(\psi[{}^3P_0]_1) &= \langle \mathcal{O}(c\bar{c}([{}^3P_0]_8) \rightarrow J/\psi) \rangle \\
 \mathcal{M}(\psi[{}^1S_0]_1) &= \langle \mathcal{O}(c\bar{c}([{}^1S_0]_8) \rightarrow J/\psi) \rangle
 \end{aligned} \tag{A1}$$

2. Indirect contribution from  $\chi_{cJ}$

$$\begin{aligned}
 \mathcal{M}(\chi[{}^3P_0]_1) &= \langle \mathcal{O}(Q\bar{Q}([{}^3P_0]_1) \rightarrow \chi_{c0}) \rangle = 3N_c \frac{|R'_{n=1}(0)|^2}{2\pi} \\
 \mathcal{M}(\chi[{}^3S_1]_8) &= \langle \mathcal{O}(Q\bar{Q}([{}^3S_1]_8) \rightarrow \chi_{c0}) \rangle
 \end{aligned} \tag{A2}$$

### 3. Indirect contribution from $\psi(2S)$

$$\begin{aligned}
\mathcal{M}(\psi[^3S_1]_1) &= \langle \mathcal{O}(c\bar{c}([^3S_1]_1) \rightarrow \psi(2S)) \rangle = 3N_c \frac{|R_{n=1}(0)|^2}{2\pi} \\
\mathcal{M}(\psi[^3S_1]_8) &= \langle \mathcal{O}(c\bar{c}([^3S_1]_8) \rightarrow \psi(2S)) \rangle \\
\mathcal{M}(\psi[^3P_0]_1) &= \langle \mathcal{O}(c\bar{c}([^3P_0]_8) \rightarrow \psi(2S)) \rangle \\
\mathcal{M}(\psi[^1S_0]_1) &= \langle \mathcal{O}(c\bar{c}([^1S_0]_8) \rightarrow \psi(2S)) \rangle
\end{aligned} \tag{A3}$$

Hence we have to determine 10 parameters. The color singlet matrix elements can be estimated from the wavefunctions of the heavy mesons. We use values from [13, 14, 49],

$$\begin{aligned}
\mathcal{M}(J/\psi[^3S_1]_1(1S)) &= 1.2\text{GeV}^3 \\
\mathcal{M}(\chi[^3P_0]_1(1P))/m_{\text{charm}}^2 &= 0.054\text{GeV}^3 \\
\mathcal{M}(\psi[^3S_1]_1(2S)) &= 0.76\text{GeV}^3.
\end{aligned} \tag{A4}$$

The color octet matrix elements can not be determined from the wavefunction because it involves the wavefunctional form of a higher Fock state. Therefore, we fit them to reproduce  $p_T$  differential cross sections at the LHC, Tevatron and RHIC. We use the following procedure to determine the remaining 6 color-octet components.

CDF [53] has measured the feed-down contribution from the  $\chi_{cJ}$  states to  $J/\psi$  production. We use this data to fit the octet matrix element  $\mathcal{M}(\chi_{c0}[^3S_1]_8)$ .

$$\mathcal{M}(\chi_{c0}[^3S_1]_8(1P))/m_{\text{charm}}^2 = (0.00187 \pm 0.00025)\text{GeV}^3, \tag{A5}$$

where the error includes the change in the matrix elements when we change the lowest  $p_T$  included in the fit by 1 GeV. The  $\chi^2/\text{dof} = 4.56$  is not very good because the (dominant) color-octet production is harder than the experimentally observed spectrum.

Similarly we assume that the measured yields of prompt  $\psi(2S)$  is not substantially contaminated by higher feed-downs and fit the following data

1. CDF results at  $\sqrt{S} = 1.96$  TeV [61] and  $\sqrt{S} = 1.8$  TeV [52, 53]
2. ATLAS results at  $\sqrt{S} = 7$  TeV [62]

We obtain,

$$\begin{aligned}
\mathcal{M}(\psi[^3S_1]_8(2S)) &= (0.0033 \pm 0.00021)\text{GeV}^3 \\
\mathcal{M}(\psi[^1S_0]_8(2S)) &= (0.0080 \pm 0.00067)\text{GeV}^3 = \mathcal{M}(\psi[^3P_0]_8(2S))/m_{\text{charm}}^2,
\end{aligned} \tag{A6}$$

with a  $\chi^2/\text{dof} = 5.6$ .

To fit the remaining fit 3 parameters we use the combined fit for the following results for  $J/\psi$  (direct+feed-down) yields

1. CDF results at  $\sqrt{S} = 1.96$  TeV [50]
2. PHENIX results at  $\sqrt{S} = 0.2$  TeV [55]
3. ATLAS results at  $\sqrt{S} = 7$  TeV [54]

Some comments regarding the fits are in order.

- Following [13, 14], we do not attempt to fit  $\mathcal{M}(\psi[^1S_0]_8)$  and  $\mathcal{M}(\psi[^3P_0]_8)/m_{\text{charm}}^2$  separately since the  $p_T$  dependence of their short distance coefficients are very similar. Therefore, we only fit a linear combination of the two parameters (we take  $\mathcal{M}(\psi[^1S_0]_8) = \mathcal{M}(\psi[^3P_0]_8)/m_{\text{charm}}^2$ ).
- The results are sensitive to the lower  $p_T$  cutoff. We do not include yields below  $p_T = 4$  GeV because using a lower cut off gives a significantly larger  $\chi^2/\text{dof}$ . The NRQCD formalism for production is expected to work well only for large  $p_T$ .
- The fits are sensitive to the sets of data considered. The ATLAS results separately prefer to have a larger  $^1S_0$  and  $^3P_j$  contribution, whereas the PHENIX results prefer the reverse. The combined fit is most similar to a fit including only CDF data.

- Additional data from STAR [56] at  $\sqrt{S} = 0.2$  TeV and CMS [73] at  $\sqrt{S} = 2.76$  TeV is consistent with our calculations and hence we don't expect them to affect the fits substantially if we include them.
- The data from TeVatron and LHC is for prompt  $J/\psi$ . RHIC data includes feed-down from  $B$ -mesons. They turn out to be unimportant at RHIC energies.

Using standard fitting techniques we find

$$\begin{aligned}\mathcal{M}(J/\psi[^3S_1]_8(1S)) &= (0.0013 \pm 0.0013)\text{GeV}^3 \\ \mathcal{M}(J/\psi[^1S_0]_8(1S)) &= (0.018 \pm 0.0087)\text{GeV}^3 = \mathcal{M}(J/\psi[^3P_0]_8(1S))/m_{\text{charm}}^2,\end{aligned}\tag{A7}$$

with a  $\chi^2/\text{dof} = 5.2$ . We also note that the uncertainty in the  $[^3S_1]$  matrix element is in particular very large, which is unfortunate because it is the dominant contribution to the total yield. The  $\chi^2/\text{dof}$  improves if we increase the lowest  $p_T$  in the fit.

With all the relevant matrix elements in hand, we can calculate production yields for all the species which contribute to the production of  $J/\psi$ , multiply by the relevant branching fractions (we ignore the small additional boost in the  $J/\psi$ ), and obtain the prompt yields for  $J/\psi$ .

To illustrate the various contributions in a specific case, we show these for the p+p baseline for LHC collisions at  $\sqrt{S} = 2.76$  TeV. The experimental data is the prompt  $J/\psi$  production yield observed at CMS [73].

In nuclear collisions, each of the species will undergo a different modification due to cold nuclear matter and quark gluon plasma effects. To obtain the p+A and A+A yields, we calculate the modified yields for each species and combine them again to obtain the net modification.

## Appendix B: Fitting color-octet matrix elements for bottomonia and a baseline for LHC at $\sqrt{S} = 2.76$ TeV

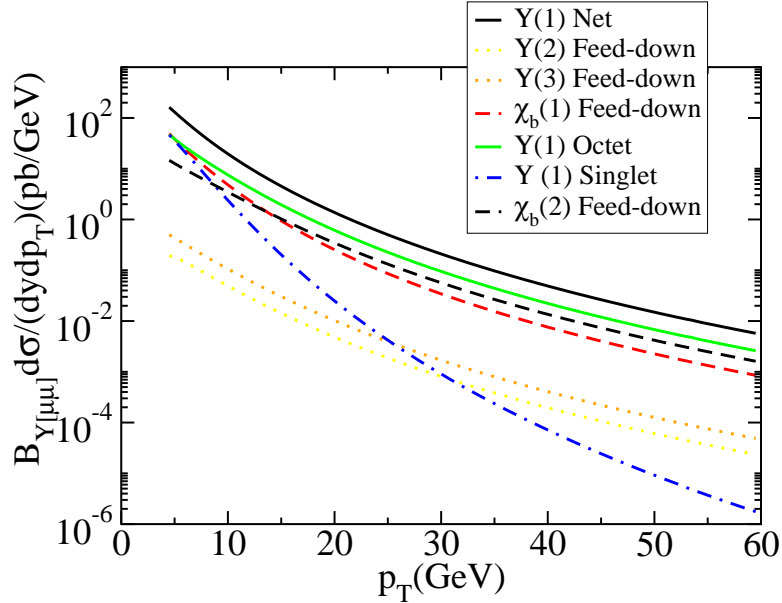


FIG. 11: (Color online) The cocktail of contributions that gives the p+p yield for  $\Upsilon(1S)$  production at the LHC at  $\sqrt{S} = 2.76$  TeV. The uppermost curve (black online) gives the net yield and gives the p+p baseline.

The analysis of  $\Upsilon(1S)$  production and feed-down contributions is very similar to the analysis for  $J/\psi$ . Following [13, 14] we consider states up to  $n = 3$ . For the  $\Upsilon(3S)$ , we consider only the direct contribution. For  $\Upsilon(2S)$ , we consider feed-down from  $\Upsilon(2S)$  and  $\chi_b(2P)$ . For  $\Upsilon(1S)$  there are additional contributions from  $\Upsilon(2S)$  and  $\chi_b(1P)$ . The relevant branching fractions are given in Table VI.

The multitude of feed-down contributions makes the fitting of the matrix elements much more subtle than for  $J/\psi$ . We use data from CDF [51] and CMS [60] to determine the matrix elements.

meson from	to $\chi_{b0}(2)$	to $\chi_{b1}(2)$	to $\chi_{b2}(2)$	to $\Upsilon(2S)$	to $\chi_{b0}(1)$	to $\chi_{b1}(1)$	to $\chi_{b2}(1)$	to $\Upsilon(1S)$
$\Upsilon(3S)$	0.131	0.126	0.059	0.199	0.003	0.0017	0.019	0.066
$\chi_{b0}(2P)$				0.046				0.009
$\chi_{b1}(2P)$				0.21				0.101
$\chi_{b2}(2P)$				0.162				0.082
$\Upsilon(2S)$					0.038	0.0715	0.069	0.267
$\chi_{b0}(1P)$								0.06
$\chi_{b1}(1P)$								0.35
$\chi_{b2}(1P)$								0.22

TABLE VI: Relevant branching fractions for bottomonia [67].

As for  $J/\psi$ , the color singlet matrix elements are estimated using the radial wavefunctions of the mesons.

$$\begin{aligned}
\mathcal{M}(\Upsilon[{}^3S_1]_1(1S)) &= 10.9\text{GeV}^3 \\
\mathcal{M}(\chi_b[{}^3P_0]_1(1P))/m_{\text{bottom}}^2 &= 0.100\text{GeV}^3 \\
\mathcal{M}(\Upsilon[{}^3S_1]_1(2S)) &= 4.5\text{GeV}^3 \\
\mathcal{M}(\chi_b[{}^3P_0]_1(2P))/m_{\text{bottom}}^2 &= 0.036\text{GeV}^3 \\
\mathcal{M}(\Upsilon[{}^3S_1]_1(3S)) &= 4.3\text{GeV}^3
\end{aligned} \tag{B1}$$

For the color-octets, we use the following procedure. We first fit the highest state,  $\Upsilon(3S)$ .

$$\begin{aligned}
\mathcal{M}(\Upsilon[{}^3S_1]_8(3S)) &= (0.0513 \pm 0.0085)\text{GeV}^3 \\
\mathcal{M}(\Upsilon[{}^1S_0]_8(3S)) &= (0.0002 \pm 0.0062)\text{GeV}^3 = \mathcal{M}(\Upsilon[{}^3P_0]_8(3S))/(5m_{\text{bottom}}^2),
\end{aligned} \tag{B2}$$

The fit of the to parameters is quite good and gives a  $\chi^2/\text{dof} = 1.33$ .

Having fixed the  $\Upsilon(3S)$  yields, we now consider  $\Upsilon(2S)$  which has feed-down from  $\Upsilon(3S)$  and from  $\chi_b(2)$ , as well as a direct production contribution. There are 4 new parameters for  $n = 2$  (the  ${}^3P_0$  and  ${}^1S_0$  are not treated as independent as in the  $J/\psi$ ). An unconstrained fit for these 4 parameters converges to an unphysical point where the direct contribution is negative and is canceled by a positive contribution from the feed-down contributions. Considering the CDF data separately does not help, and a problem of similar nature appears in fitting the CMS data, albeit with the  $\chi_b$  contribution. As expected, letting the  ${}^1S_0$  and  ${}^3P_0$  matrix elements free to float does not help with the fitting because the shapes of the two contributions is very similar.

To resolve this issue, we limit the variation in the  ${}^3S_1$  contribution by assuming that it roughly scales with mass in going from  $J/\psi$  to  $\Upsilon(2S)$ .

$$\begin{aligned}
\mathcal{M}(\Upsilon[{}^3S_1]_8(2S)) &\in \left[\frac{1}{10}, 10\right] \times \mathcal{M}(J/\psi[{}^3S_1]_8(1S)) \left(\frac{m_{\Upsilon(2S)}}{m_{\psi(1S)}}\right)^3 \\
\mathcal{M}(\chi_b[{}^3S_1]_8(2P)) &\in \left[\frac{1}{10}, 10\right] \times \mathcal{M}(\chi_c[{}^3S_1]_8(1P)) \left(\frac{m_{\chi_b(2P)}}{m_{\chi_c(1P)}}\right)^3
\end{aligned} \tag{B3}$$

With these assumptions, the 5 matrix elements can be fit while satisfying the constraint that production cross sections for all the particles are positive. To obtain an error estimate, we fit the LHC and CDF data separately, and the difference gives an estimate of the variation in the parameters. The results obtained are as follows,

$$\begin{aligned}
\mathcal{M}(\Upsilon[{}^3S_1]_8(2S)) &= (0.0224 \pm 0.0196)\text{GeV}^3 \\
\mathcal{M}(\Upsilon[{}^1S_0]_8(2S)) &= (-0.0067 \pm 0.0084)\text{GeV}^3 = \mathcal{M}(\Upsilon[{}^3P_0]_8(2S))/(5m_{\text{bottom}}^2) \\
\mathcal{M}(\chi_b[{}^3S_1]_8(2P)) &= (0.0324)\text{GeV}^3.
\end{aligned} \tag{B4}$$

Note that having  ${}^1S_0$  contributions to be negative is not a problem. The main physical requirement is that the net cross sections should be positive for all  $p_T$ . The quality of the fit is worse than the fit for  $\Upsilon(3S)$ , with a  $\chi^2/\text{dof} = 3.5$ . In particular the yields at CDF are underpredicted. Perhaps including higher order corrections in  $\alpha_s$ , and more data can improve the fit in the future. We also comment on the fact that we don't quote an error estimate for the  $\chi_b(2P)$  matrix element in Eq. B4. In our fitting procedure, the  $\mathcal{M}(\chi_b[{}^3S_1]_8(2P))$  converges to the boundary of the constrained region in Eq. B3 for both LHC and CDF data. Hence a trustworthy error estimate can not be obtained in this case. A similar situation arises for the fitting of the  $\Upsilon(3S)$  matrix elements.

Next we consider the production of  $\Upsilon(1S)$ . We handle the  $^3S_1$  components in the same way as for  $\Upsilon(2S)$ . The results are given below,

$$\begin{aligned}\mathcal{M}(\Upsilon[^3S_1]_8(1S)) &= (0.0477 \pm 0.0334)\text{GeV}^3 \\ \mathcal{M}(\Upsilon[^1S_0]_8(1S)) &= (0.0121 \pm 0.040)\text{GeV}^3 = \mathcal{M}(\Upsilon[^3P_0]_8(1S))/(5m_{\text{bottom}}^2) \\ \mathcal{M}(\chi_b[^3S_1]_8(1P)) &= (0.1008)\text{GeV}^3.\end{aligned}\tag{B5}$$

The  $\chi^2/\text{dof} = 3.8$ .

Some comments regarding the fits are in order.

- Following [13, 14], we do not attempt to fit  $\mathcal{M}(\Upsilon[^1S_0]_8(nS))$  and  $\mathcal{M}(\Upsilon[^3P_0]_8(nS))/m_{\text{bottom}}^2$  separately since the forms of their short distance pieces are very similar. Therefore, we only fit a linear combination of the two parameters (we take  $\mathcal{M}(\Upsilon[^1S_0]_8(nS)) = \mathcal{M}(\Upsilon[^3P_0]_8(nS))/(5m_{\text{bottom}}^2)$  which is the relative scale of the two contributions).
- The results are sensitive to the lower  $p_T$  cutoff. We do not include yields below  $p_T = 5$  GeV.

### Appendix C: $B$ feed-down contribution

Using previous results for the production of  $B$ -hadrons [31] and calculating their decay to  $J/\psi$ , we have estimated the feed-down contribution from  $B$ -hadrons to the  $J/\psi$  yields. Our model for  $B$ -decay gives results that give the right trend when compared with the observations from CDF and ATLAS. At RHIC we find that at least up to  $p_T \sim 20$  GeV, the feed-down contribution is smaller than the prompt production but is not insignificant. We attribute this fact partly to the hardness of the NRQCD spectrum.

### Appendix D: Results for $J/\psi$ production at forward rapidity $y = 3$

While this paper focuses on results for quarkonium production and modification relevant to the central rapidity region at the LHC, it is useful to investigate the implications of our theoretical model for forward rapidity. In this example, we select  $y = 3$  and evaluate the  $J/\psi$  production cross section in p+p, p+Pb and Pb+Pb reactions. We are motivated by the possibility that the ALICE experiment [75] will soon measure such cross sections up to a high transverse momentum.

Due to the large center-of-mass energy per nucleon pair and the wide rapidity range at the LHC, the steepness of the underlying quarkonium production cross sections does not differ considerably between  $y = 0$  and  $y = 3$ . Cold nuclear matter effects are expected to be qualitatively similar for these 2 rapidities. Furthermore, the charged particle rapidity density, which is proportional to the QGP density in the Bjorken expansion scenario, is expected to vary by less than 20% over the rapidity range of interest. In the co-moving plasma frame (in our case this means boosting to  $y = 3$ ), quarkonia propagate strictly in the transverse direction. Thus, the final-state dynamics at forward rapidity in the Bjorken expansion scenario is described by the same set of equations that we used to obtain the mid-rapidity results as long as one is careful to use transverse sizes and transverse momenta.

Our results of the high- $p_T$   $J/\psi$  suppression at  $y = 3$  are presented in Fig. 13. The conventions in the plots are the same as in Section VI.

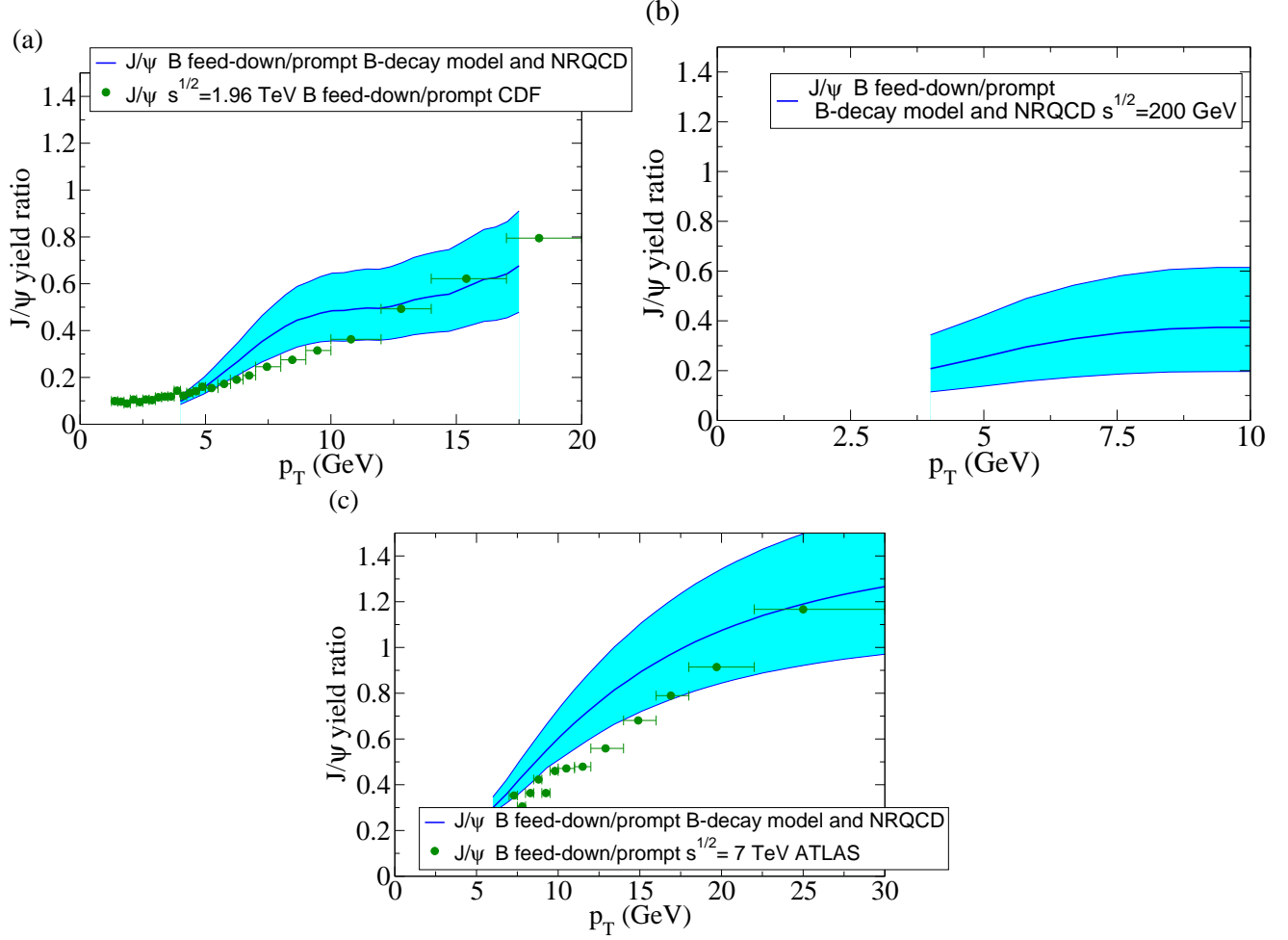


FIG. 12: (Color online) Ratio of the  $J/\psi$  yield from  $B$  feed-down to the prompt yield. The upper left panel corresponds to data for the yield of  $J/\psi$  from CDF at  $\sqrt{S} = 1.96$  TeV [50]. The upper right panel is for RHIC at  $\sqrt{S} = 0.2$  TeV. The bottom panel has data from the LHC at  $\sqrt{S} = 7$  TeV from the ATLAS collaboration [54]. The darker colored error bars (dark green online) show the experimental results for the ratio and the error bar represents the width of the larger energy bin of the prompt and  $B$  feed-down yield. The solid line (blue online) is the theoretically calculated result. The uncertainty band is associated with the scale variation in the production of  $J/\psi$ , as in Fig. 1. Uncertainties in the  $B$ -feeddown are not displayed.

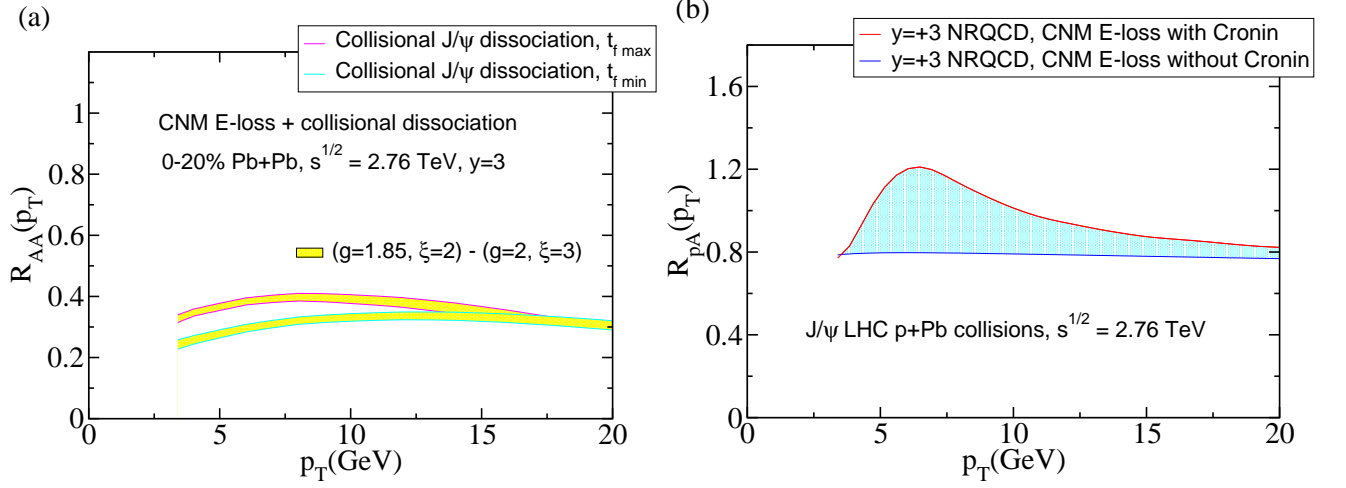


FIG. 13: (Color online) Results for  $R_{AA}$  (left panel) and  $R_{pA}$  right panel at  $y = 3$  where positive rapidity corresponds to motion parallel to the proton in p+A collisions. We only show results for  $R_{AA}$  ignoring the Cronin effect. One can constrain the Cronin effect from experiments by comparing with  $R_{pA}$  for  $y = 3$ .

- 
- [1] T. Matsui and H. Satz, Physics Letters B, **178** (1986), 416-422.
- [2] A. Mocsy and P. Petreczky, Phys. Rev. Lett. **99**, 211602 (2007).
- [3] F. Karsch and H. Satz, Zeitschrift für Physik C Particles and Fields, **51** 2 (1991), 209.
- [4] F. Karsch, D. Kharzeev, H. Satz, Physics Letters B, **637** (2006), 75-80.
- [5] Z. Conesa del Valle *et al.*, Nucl. Phys. Proc. Suppl. **214**, 3 (2011).
- [6] X. Zhao and R. Rapp, [arXiv:0806.1239 [nucl-th]].
- [7] C. Lourenço, R. Vogt and H. K. Wöhri, Journal of High Energy Physics, **02**, 014 (2009).
- [8] R. Rapp and H. van Hees, [arXiv:0903.1096 [hep-ph]].
- [9] M. Strickland, Phys. Rev. Lett. **107**, 132301 (2011) and M. Strickland and D. Bazow, Nuclear Physics A **879** (2012), 25-58.
- [10] M. Margotta, K. McCarty, C. McGahan, M. Strickland and D. Yager-Elorriaga, Phys. Rev. D **83**, 105019 (2011) [Erratum-ibid. D **84**, 069902 (2011)].
- [11] T. Song, K. C. Han and C. M. Ko, Phys. Rev. C **85**, 014902 (2012).
- [12] G. T. Bodwin, E. Braaten and G. P. Lepage, Phys. Rev. D **51**, 1125 (1995) [Erratum-ibid. D **55**, 5853 (1997)].
- [13] P. L. Cho and A. K. Leibovich, Phys. Rev. D **53**, 6203 (1996).
- [14] P. L. Cho and A. K. Leibovich, Phys. Rev. D **53**, 150 (1996).
- [15] E. Braaten, S. Fleming and A. K. Leibovich, Phys. Rev. D **63**, 094006 (2001).
- [16] F. Cooper, M. X. Liu and G. C. Nayak, Phys. Rev. Lett. **93**, 171801 (2004) and G. C. Nayak, M. X. Liu and F. Cooper, Phys. Rev. D **68**, 034003 (2003).
- [17] Z. B. Kang, J. W. Qiu, and G. Sterman. Phys. Rev. Lett. **108**, 102002 (2012).
- [18] R. Vogt, Phys. Rev. C **81**, 044903 (2010).
- [19] I. Vitev, Phys. Lett. B **562** (2003), 36.
- [20] M. Gyulassy, I. Vitev, X. N. Wang and B. W. Zhang, [arXiv:nucl-th/0302077].
- [21] J. W. Qiu and I. Vitev, Phys. Rev. Lett. **93**, 262301 (2004).
- [22] J. W. Qiu and I. Vitev, Phys. Lett. B **632** (2006), 507.
- [23] I. Vitev, Physics Letters B **639**, Issue-1 (2006), 38-45.
- [24] I. Vitev, Phys. Rev. C **75**, 064906 (2007).
- [25] R. B. Neufeld, I. Vitev and B. -W. Zhang, Phys. Lett. B **704** (2011), 590.
- [26] Z. B. Kang, I. Vitev, and H. Xing. Phys. Rev. D **85** 054024, (2012).
- [27] I. Vitev and B. W. Zhang, Phys. Lett. B **669** (2008), 337.
- [28] I. Vitev, T. Goldman, M. B. Johnson and J. W. Qiu, Phys. Rev. D **74**, 054010 (2006) [hep-ph/0605200].
- [29] Z. B. Kang and I. Vitev, Phys. Rev. D **84**, 014034 (2011).
- [30] A. Accardi, [arXiv:hep-ph/0212148] and references therein.
- [31] A. Adil and I. Vitev, Phys. Lett. B **649**, 139 (2007).
- [32] R. Sharma, I. Vitev and B. W. Zhang, Phys. Rev. C **80**, 054902 (2009).
- [33] O. Kaczmarek and F. Zantow, Phys. Rev. D **71**, 114510 (2005).
- [34] M. Laine, O. Philipsen, P. Romatschke and M. Tassler, JHEP **0703** (2007) 054.
- [35] N. Brambilla, J. Ghiglieri, A. Vairo and P. Petreczky, Phys. Rev. D **78**, 014017 (2008), M. A. Escobedo, J. Soto and M. Mannarelli, Phys. Rev. D **84**, 016008 (2011) and references therein.
- [36] Y. Park, K. -I. Kim, T. Song, S. H. Lee and C. -Y. Wong, Phys. Rev. C **76**, 044907 (2007). T. Song, Y. Park, S. H. Lee, C. -Y. Wong, Physics Letters B **659** (2008), 621.
- [37] M. E. Peskin, Nucl. Phys. B **156**, 365 (1979).
- [38] J. Casalderrey-Solana, H. Liu, D. Mateos, K. Rajagopal and U. A. Wiedemann, [arXiv:1101.0618]
- [39] F. Dominguez and B. Wu, Nucl. Phys. A **818**, 246 (2009).
- [40] F. Dominguez, C. Marquet and B. Wu, Nucl. Phys. A **823** 99-119(2009).
- [41] A. Knospe, [arXiv:1201.0242]
- [42] A. Adare *et al.* [PHENIX Collaboration], Phys. Rev. Lett. **98**, 172301 (2007).
- [43] B. I. Abelev *et al.* [STAR Collaboration], Phys. Rev. Lett. **98**, 192301 (2007) [Erratum-ibid. **106**, 159902 (2011)].
- [44] A. Dainese, J. Phys. G **38**, 124032 (2011).
- [45] S. A. Bass, J. Phys. Conf. Ser. **50** 279, (2006).
- [46] A. D. Martin, W. J. Stirling, R. S. Thorne and G. Watt, Eur. Phys. J. C **63** 189-285 (2009)
- [47] R. Baier and R. Rückl, Zeitschrift für Physik C Particles and Fields, 0170-9739, **19**, 3, 251-266 (1983).
- [48] B. Humpert, Phys. Lett. B, **184**, Issue 1, 105-107 (1987).
- [49] E. J. Eichten and C. Quigg, Phys. Rev. D **49** 5845 (1994).
- [50] D. Acosta *et al.* [CDF Collaboration], Phys. Rev. D **71**, 032001 (2005).
- [51] D. Acosta *et al.* [CDF Collaboration], Phys. Rev. Lett. **88**, 161802 (2002).
- [52] Abe, F., *et al.* [CDF Collaboration] Phys. Rev. Lett. **79**, 572 (1997).
- [53] F. Abe *et al.* [CDF Collaboration], Phys. Rev. Lett. **79**, 578 (1997).
- [54] G. Aad *et al.* [ATLAS Collaboration], Nucl. Phys. B **850**, 387 (2011).
- [55] A. Adare *et al.* [PHENIX Collaboration], Phys. Rev. D **82**, 012001 (2010).
- [56] B. I. Abelev *et al.* [STAR Collaboration], Phys. Rev. C **80**, 041902 (2009).

- [57] M. Butenschon and B. A. Kniehl, Phys. Rev. Lett. **106**, 022003 (2011).
- [58] M. Butenschoen and B. A. Kniehl, Phys. Rev. D **84**, 051501 (2011).
- [59] M. Butenschoen and B. A. Kniehl, Phys. Rev. Lett. **107**, 232001 (2011).
- [60] V. Khachatryan *et al.* [CMS Collaboration], Phys. Rev. D **83**, 112004 (2011).
- [61] T. Aaltonen *et al.* [CDF Collaboration], Phys. Rev. D **80**, 031103 (2009).
- [62] S. Chatrchyan *et al.* [CMS Collaboration], [arXiv:1111.1557 [hep-ex]]
- [63] P. R. Norton, Reports on Progress in Physics, **66** (2003), 1253-1297.
- [64] K.J. Eskola, V.J. Kolhinen and C.A. Salgado, Eur. Phys. J. C, **9** 61-68 (1999)
- [65] G. Ovanesyan and I. Vitev, Phys. Lett. B **706**, 371 (2012).
- [66] C. Markert, R. Bellwied and I. Vitev, Phys. Lett. B **669**, 92 (2008).
- [67] K. Nakamura *et al.* (Particle Data Group), J. Phys. G**37**, 075021 (2010).
- [68] I. Vitev, S. Wicks and B. -W. Zhang, JHEP **0811**, 093 (2008).
- [69] R. B. Neufeld, I. Vitev and B. -W. Zhang, Phys. Rev. C **83**, 034902 (2011).
- [70] Dokshitzer, Y. L., and D. E. Kharzeev. Physics Letters B **519** (2001), 199-206.
- [71] M. Djordjevic and M. Gyulassy, Nucl. Phys. A **733**, 265 (2004)
- [72] Z. Tang [STAR Collaboration], J. Phys. G **38**, 124107 (2011).
- [73] S. Chatrchyan *et al.* [CMS Collaboration], [arXiv:1201.5069]
- [74] G. Aad *et al.* [Atlas Collaboration], Phys. Lett. B **697** (2011) 294.
- [75] B. Abelev *et al.* [ALICE Collaboration], [arXiv:1202.1383 [hep-ex]].
- [76] S. Chatrchyan *et al.* [CMS Collaboration], Phys. Rev. Lett. **107**, 052302 (2011).
- [77] R. Reed [STAR Collaboration], J. Phys. Conf. Ser. **270**, 012026 (2011) [Nucl. Phys. A **855**, 440 (2011)]; Quark Matter 2011.
- [78] M. Gyulassy, P. Levai, and I. Vitev, Phys. Rev. D **66**, 014005 (2002).
- [79] A. Adare, S. Afanasiev, C. Aidala, N. N. Ajitanand, Y. Akiba, H. Al-Bataineh, J. Alexander and A. Angerami *et al.*, arXiv:1204.0777 [nucl-ex].